Dust Content Modulation and Spring Heat Waves in Senegal (2003–2022)

Semou Diouf, Marie-Jeanne Sambou, Abdoulaye Deme, Papa Fall, Dame Gueye, Juliette Mignot, Serge Janicot

atmosphere

MDPI

Article

Dust Content Modulation and Spring Heat Waves in Senegal (2003–2022)

Semou Diouf [1], Marie-Jeanne G. Sambou [2], Abdoulaye Deme [1,*], Papa Fall [1], Dame Gueye [1], Juliette Mignot [3] and Serge Janicot [3]

[1] Laboratoire Environnement, Ingénierie, Télécommunications et Energies Renouvelables (LEITER), Unité de Formation et de Recherche de Sciences Appliquées et de Technologie, Université Gaston Berger (UGB), Saint-Louis 32000, Senegal; diouf.semou3@ugb.edu.sn (S.D.); fall.papa@ugb.edu.sn (P.F.); gueye.dame2@ugb.edu.sn (D.G.)

[2] Laboratoire de Physique de l'Atmosphère et de l'Océan–Siméon Fongang (LPAOSF), Ecole Supérieure Polytechnique, Université Cheikh Anta Diop (UCAD), Dakar 10700, Senegal; marie.sambou@ucad.edu.sn

[3] Laboratoire d'Océanographie et du Climat: Expérimentations et Approches Numériques (LOCEAN), Sorbonne Université (UPMC), IRD, CNRS, 75005 Paris, France

* Correspondence: abdoulaye.deme@ugb.edu.sn; Tel.: +221-77-804-91-62

Abstract: The population of Senegal faces health challenges related to desert dust and heat waves (HWs). This study aims to (a) update the documentation of HWs in Senegal, expanding on the work of Sambou et al. (2019); (b) investigate the modulation of dust indicators during HWs; and (c) assess the distinct impacts of dust content on night-time and daytime HWs. We use [i] the daily maximum air temperature (Tx), minimum air temperature (Tn), and apparent temperature (Ta) from 12 stations in the Global Surface Summary of the Day (GSOD) database and [ii] the Dust Aerosol Optical Depth (Dust AOD), particulate matter (PM) concentrations, 925 hPa wind, and Mean Sea Level Pressure (MSLP) from the Copernicus Atmosphere Monitoring Service (CAMS) reanalysis. HWs are defined for each station in spring as periods when Tx, Tn, or Ta exceeds the 95th percentile for at least three consecutive days. Three homogeneous zones from the Atlantic coast to inland Senegal are identified using hierarchical cluster analysis: Zone 1 (Saint-Louis, Dakar-Yoff, Ziguinchor, and Cap Skirring), Zone 2 (Podor, Linguère, Diourbel, and Kaolack), and Zone 3 (Matam, Tambacounda, Kédougou, and Kolda). Our results show that Zone 1 records the highest number of HWs for Tx, Tn, and Ta, while Zone 3 experiences more HWs in terms of Tn and Ta than Zone 2. The influence of dust is notably stronger for HWs linked to Tn and Ta than for those related to Tx. Analysis of the mechanisms shows that the presence of dust in Senegal and its surrounding regions is detected up to four days before the onset of HWs. These findings suggest that dust conditions associated with spring HWs in Senegal may be better distinguished and predicted.

Keywords: heat waves; dust; GSOD; CAMS; Senegal

Citation: Diouf, S.; Sambou, M.-J.G.; Deme, A.; Fall, P.; Gueye, D.; Mignot, J.; Janicot, S. Dust Content Modulation and Spring Heat Waves in Senegal (2003–2022). *Atmosphere* **2024**, *15*, 1413. https://doi.org/10.3390/atmos15121413

Academic Editor: Luca Stabile

Received: 19 October 2024
Revised: 18 November 2024
Accepted: 22 November 2024
Published: 25 November 2024

1. Introduction

The Sahel faces significant climatic challenges, which are being exacerbated by climate change. Heat waves (HWs) and dust storms are among the extreme events impacting this region. The scientific community widely recognizes that the Earth is undergoing global warming, primarily driven by the increase in greenhouse gas emissions due to human activities [1,2]. This warming trend is accompanied by persistent changes in climate extremes, including increases in the frequency, duration, and intensity of HWs [3–5].

Climate projections suggest that the likelihood of HWs will double with a global temperature increase of +2 °C compared to +1.5 °C and will be five times higher than under the current temperature conditions [6].

HWs raise serious concerns due to their significant impacts on various sectors, particularly public health [7,8]. Numerous studies have documented the dramatic health

consequences of HWs in North America and Europe over the past two decades, including the July 1995 HW in Chicago, which resulted in over 600 deaths [9]; the 2003 HW in Europe, which claimed 70,000 lives [10]; and the Russian HW in 2010, which caused more than 11,000 deaths [11]. Similarly, severe HWs have been recorded in the Sahel in recent years. In April 2010, Niamey experienced nearly 40 deaths per day, especially among children and the elderly, while, in April 2024, Kayes (Mali) saw multiple fatalities in the capital, with record temperatures reaching 48.5 °C [12]. Senegal was particularly affected by HWs in 2010 and in late May of 2013 (from the 24th to the 27th), especially in its northern regions (Matam, Bakel, and Podor), where air temperatures exceeded 45 °C, leading to several deaths [13,14].

In addition to extreme temperatures, another critical factor in the context of global climate is the significant presence of aerosols. The latter—particularly mineral dust—are one of the major sources of uncertainty regarding radiative forcing in the climate system [15]. North Africa is the largest source of mineral aerosols worldwide. The main source regions (hotspots) include the foothills of the Atlas Mountains, northwestern Mali, eastern Mauritania, southern Algeria, eastern Niger, Chad, and the eastern Libyan desert, as well as vast areas of Egypt and Sudan (Nubian Desert) [16,17]. The northeast-to-southwest trade winds—notably the Harmattan during winter and spring—along with convective processes in summer, facilitate the emission and transport of substantial quantities of mineral dust into the atmosphere [18]. In winter, the Harmattan winds primarily move southward, carrying around 60% of the annual Saharan dust towards the Gulf of Guinea [19], with some particles even reaching South America [20] and the Caribbean [21]. During summer, the monsoon flow and cyclonic activity transport dust at higher altitudes [22], thus steering the dust plume westward, with approximately 12% of the annual dust reaching the Atlantic Ocean [19].

Dust aerosols account for nearly 30% of the global Aerosol Optical Depth (AOD) and over 70% of the total aerosol mass loading [23]. These suspended particles play a crucial role in Earth's climate system, influencing climate dynamics, biogeochemical cycles, and other Earth system processes [24–26]. Dust aerosols affect both shortwave and longwave radiative fluxes through the scattering and absorption of radiation [27]. In the shortwave spectrum, dust particles scatter and reflect incoming solar radiation, reducing the amount of energy reaching the Earth's surface. This cooling effect is particularly pronounced over bright surfaces such as deserts and oceans, where the contrast in albedo enhances the scattering process. The net radiative forcing from this scattering at the top of the atmosphere is estimated to be around $-0.3\ W/m^2$, with significant regional variations [28]. Conversely, in the longwave spectrum, dust particles absorb and re-emit infrared radiation, leading to atmospheric warming, especially in the lower atmospheric layers. This process can significantly influence atmospheric dynamics and stability [29]. Recent studies have highlighted the feedback effects of direct radiative forcing from dust on precipitation deficits [30] and substantial warming of both the Earth's surface and upper atmosphere [31]. The frequency and intensity of sandstorms have increased in recent decades, particularly in the Middle East, Southwest Asia, and the Sahel. Notable events include sandstorms in the Middle East and Pakistan in 2012 and 2015, as well as a severe dust storm over the Sahara from 14 to 19 June 2020, which was considered the most intense since 2002 [32].

The health of populations in sub-Saharan Africa is severely impacted not only by global warming—which is increasing at a rate higher than the global average—but also by more frequent, prolonged, and intense HWs, as well as exposure to outdoor air pollution [33,34]. Particles larger than 10 µm primarily affect external organs, leading to skin irritation, conjunctivitis, and eye infections. In contrast, particles smaller than 10 µm, such as most desert dust, can be inhaled, causing respiratory problems such as asthma, tracheitis, pneumonia, allergic rhinitis, and silicosis [35,36]. Ultrafine particles, when they reach the lower respiratory tract, can impact the internal organs and trigger cardiovascular problems. Furthermore, certain infectious diseases, such as meningococcal meningitis, are also transmitted via dust [37,38], as inhaling dust particles during hot, dry periods irri-

tates the nasal mucous membranes, increasing susceptibility to bacterial infections [39,40]. A global model assessment estimated that, in 2014, exposure to dust particles resulted in 400,000 premature deaths due to cardiopulmonary diseases among individuals over 30 years of age [41]. In sub-Saharan Africa, according to the World Health Organization (WHO), around 456,000 deaths were linked to ambient air pollution in 2016, with related deaths rising rapidly in recent years [42,43]. Researchers have estimated that, in 2020, about 9 million people died annually (accounting for 12% of all deaths) due to exposure to air pollution, leading to a global average decrease in life expectancy of nearly three years [44]. Exposure to PM2.5 is highest in Africa [45], and children aged 5–15 years are five times more likely to die from air pollution-related causes than their counterparts in low- and middle-income countries in Southeast Asia [46]. In Dakar, Senegal, observations of PM10 and PM2.5 from 2013 to 2016 revealed numerous instances of unhealthy and hazardous PM levels during the winter season [47]. According to these studies, dust simulations indicate that northern Senegal experiences the highest concentrations of PM2.5 and PM10 during the winter, with some administrative districts being particularly affected.

HWs and dust storms are two major hazards in the Sahel region, which can independently or concurrently expose vulnerable and fragile populations to significant health risks due to poverty and limited adaptive capacity and access to healthcare. Therefore, it is crucial to understand the connections between HWs and dust episodes in order to better anticipate and mitigate the harmful impacts of these extreme climatic events. There are still uncertainties regarding the relationships between air pollution, global warming, and associated health risks, which is why recent research has focused on this area globally. For instance, in Portugal, Valenzuela et al. [48] analyzed the influence of the extreme Sahara desert dust event from 4 to 7 April 2011 on shortwave and longwave radiation. They found that an increase in Aerosol Optical Depth (AOD) was linked to a radiative cooling effect at short wavelengths, counterbalanced by a warming effect at the surface due to longwave radiation. Similarly, Souza et al. [49] demonstrated that the HWs in Spain during 2018 and 2019 were exacerbated by the intrusion of a warm air mass associated with higher-than-normal concentrations of Saharan dust, which contributed to an increase in surface temperatures. Conversely, research by Diba et al. [50] indicated that mineral particles have the potential to mitigate HWs, especially during spring and summer, particularly in the northern Sahel. However, a recent study by Niane et al. [51] assessed the impact of mineral dust on spring HWs in the Sahel, and found evidence of a potential local warming effect, in contrast with the earlier findings of Diba et al. [50].

Although the links between HWs and dust have been studied on a regional scale in the Sahel, no specific study addressing this issue in Senegal has been published to date. However, recent research on HWs has indicated that Senegal exhibits unique characteristics compared to the rest of the Sahel, largely due to its location as the westernmost point of Africa [52]. Sambou et al. [52] identified three key findings that are particularly relevant for understanding the role of dust content modulation: (i) Unlike HWs in the central Sahel, the primary pattern controlling HWs in Senegal is characterized by positive pressure anomalies centered around the Strait of Gibraltar, which promote easterly to northeasterly wind anomalies. (ii) Senegal can be divided into three homogeneous zones (Zone 1, Zone 2, and Zone 3), each comprising four stations from west (Atlantic coastline) to east (inland Senegal). In these zones, temperature and moisture patterns shift eastward, while pressure anomalies decrease significantly. (iii) There is a notable difference between night-time HWs (linked to minimum temperatures) and daytime HWs (linked to maximum temperatures). Night-time HWs were found to be associated with higher water vapor content than daytime HWs, corroborating and expanding upon previous findings over the Sahel.

These findings suggest that further investigation into the relationship between dust and HWs in Senegal is warranted, especially in the context of climate change, where disparities between the western Sahel and the rest of the Sahel are becoming more pronounced.

The aim of this study is to update the documentation of HWs over Senegal during the recent period, building on the work of Sambou et al. [52]. Additionally, we investigate the

modulation of dust indicators and their associated synoptic-scale atmospheric patterns. Furthermore, we explore the hypothesis that variations in dust content distinctly influence the characteristics of night-time HWs (associated with minimum air temperature) and daytime HWs (associated with maximum air temperature) in Senegal.

2. Materials and Methods

2.1. Study Area

Senegal (12–17° N, 18–11° W), located at the westernmost point of Africa, is bordered by the Atlantic Ocean (Figure 1). The country experiences two distinct seasons: The rainy season, from June to October, also known as the wintering season, typically begins in the southeast and gradually extends northward. Rainfall increases gradually until it peaks in mid-August, after which it sharply decreases from mid-September and becomes increasingly scarce by October [53]. The second season, from November to May, is characterized by a dry climate, with average temperatures ranging between 22 °C and 36 °C. There are significant temperature variations between the coastal areas and the interior. According to the Köppen–Geiger climate classification, Senegal is divided into three major climatic zones, following a north–south gradient [54]: (i) Arid, Desert, Hot (BWh): this zone, characterized by a semi-arid or arid climate, includes the stations of Saint-Louis, Podor, Linguère, and Matam; (ii) Arid, Steppe, Hot (BSh): this zone includes the stations of Dakar-Yoff, Diourbel, Kaolack, and Tambacounda; and (iii) Tropical, Savannah (Aw): this zone encompasses the stations of Cap Skirring, Ziguinchor, Kolda, and Kédougou.

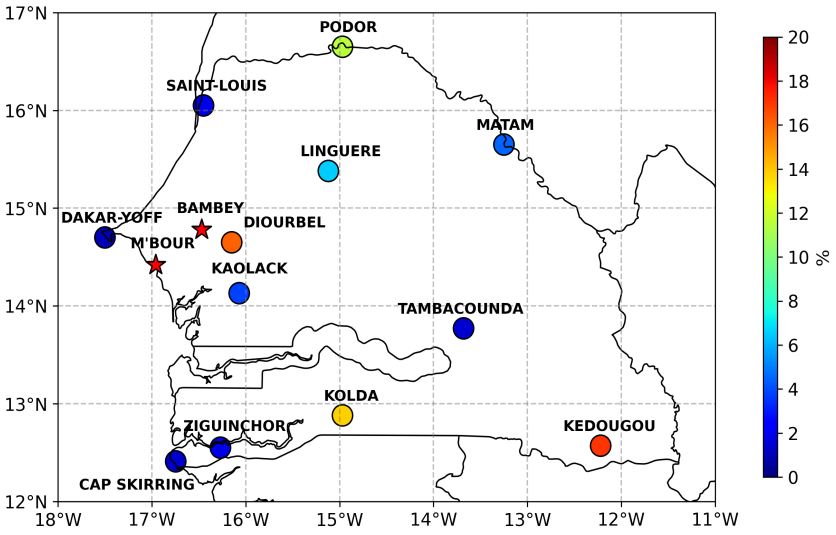

Figure 1. Map of Senegal with 12 synoptic stations from GSOD (Global Surface Summary of the Day). Colors indicate percentage of missing data at stations. Red stars mark the locations of the Sahelian Dust Transect stations: M'Bour (16.96° W, 14.39° N) and Bambey (16.47° W, 14.70° N) (see Section 2.3.2).

2.2. In Situ Temperature Data Set from GSOD

The observational climate temperature data used in this study were extracted from the GSOD (Global Surface Summary of the Day) database, which includes 18 daily surface meteorological variables. These variables include daily maximum air temperature (Tx), minimum air temperature (Tn), average air temperature measured at 2 m (T2m), and dew point temperature (Td). Using T2m and Td, we calculated the apparent temperature (Ta) using the formula outlined by [52] and previously applied by [55]:

$$Ta = -2.653 + 0.994 \times T2m + 0.0153 \times Td^2. \quad (1)$$

The temperature data used in this study were obtained from 12 stations across Senegal (Dakar-Yoff, Cap Skirring, Diourbel, Kaolack, Podor, Linguère, Matam, Kédougou, Saint-

Louis, Tambacounda, Kolda, and Ziguinchor) for the period from 2003 to 2022, as shown in Figure 1. These observational data exhibit gaps, with varying proportions across the 12 stations (ranging from 1% to 20%). Before analysis, missing data were imputed using the MissForest method, which is recognized for its effectiveness in imputing time-series temperature data [56,57].

2.3. Aerosol Data Sets from In Situ Measurements and Reanalysis

2.3.1. PurpleAir Data Set

Data on fine particulate matter concentrations with diameters less than 2.5 µm (PM2.5) and less than 10 µm (PM10) were collected using the PurpleAir sensor network deployed in the city of Saint-Louis, as part of the Jeune Équipe Associée à l'IRD Climat et Santé au Sénégal (JEAI-CLISAS) project. The main objective of JEAI-CLISAS is to provide tools and methods to detect, prevent, inform, and act on the health impacts of hazardous climatic events (e.g., heat waves, dust events) in northern Senegal.

The effects of desert dust episodes were taken into account by combining them with the specific characteristics of the urban context of the Saint-Louis area, such as the heat island effect and urban pollution. The sensors used were PurpleAir PA-II-FLEX (see https://www2.purpleair.com/products/purpleair-flex for more details, accessed on 21 March 2024), installed at 13 colleges and carefully distributed in the area to capture a range of environmental conditions and air pollution levels. These colleges include Abdoulaye Mar Diop Middle School (AMD), Samba Ndieme Sow Middle School (SNS), and Ameth Fall Secondary School (AF) located on the island. In Sor, there are Ameth Telemaque Sow Middle School (ATS), Andre Peytavin Middle School (AP), and Sankore Private Course (SPC). Towards the Pikine zone, we have Pikine Middle School (PM), Guinaw Rail Middle School (GR), and Augustin Henry Louis Guillabert Secondary School (AHLG). Finally, Ngallele Middle School (NM), Ngallele-Bango Middle School (NB), Bango Middle School (BM), and Samba Lampsar Private Course (SLP) complete the list (see Figure 2). Data were collected over the period 2021–2022. The GR and SLP data were ultimately not utilized due to a high percentage of missing data.

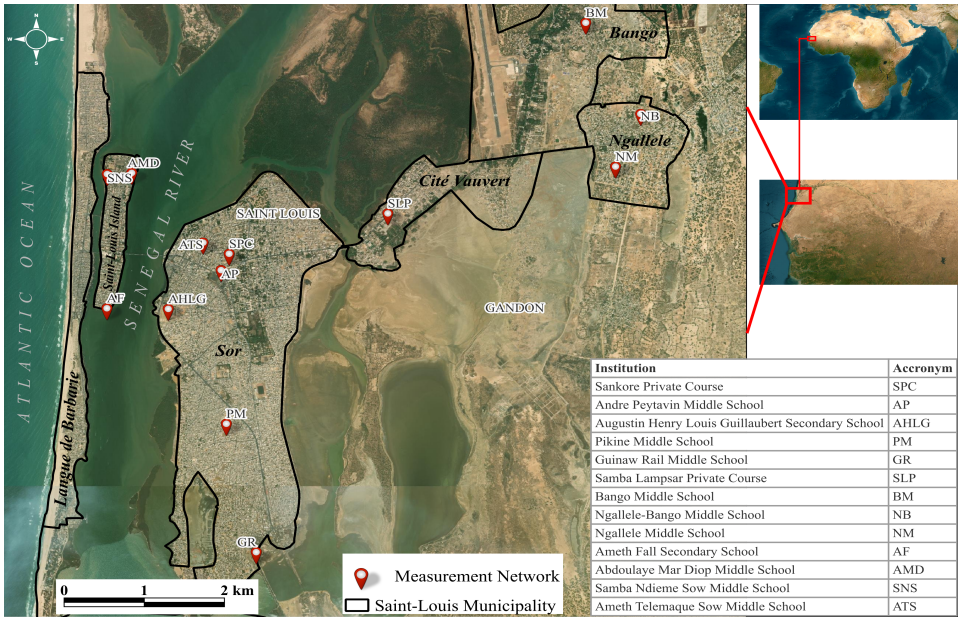

Institution	Accronym
Sankore Private Course	SPC
Andre Peytavin Middle School	AP
Augustin Henry Louis Guillaubert Secondary School	AHLG
Pikine Middle School	PM
Guinaw Rail Middle School	GR
Samba Lampsar Private Course	SLP
Bango Middle School	BM
Ngallele-Bango Middle School	NB
Ngallele Middle School	NM
Ameth Fall Secondary School	AF
Abdoulaye Mar Diop Middle School	AMD
Samba Ndieme Sow Middle School	SNS
Ameth Telemaque Sow Middle School	ATS

Figure 2. Location of PurpleAir sensors for the Jeune Équipe Associée à l'IRD Climat et Santé au Sénégal (JEAI-CLISAS) project. The names and acronyms of colleges are shown in the bottom right of the figure.

In this study, we used the PM2.5 and PM10 variable with the correction factor (CF) set to ATM. The ATM correction factor is applied to adjust these measurements to account for outdoor environmental conditions, ensuring a more accurate data representation [58].

2.3.2. INDAAF Data Set

INDAAF (International Network for the Study of Deposition and Atmospheric Composition in Africa) is a network dedicated to studying atmospheric composition and deposition fluxes across Africa. It was formed in 2015 through the merger of two pre-existing entities: the IDAF observation service (IGAC-DEBITS Africa) and the "Sahelian Dust Transect" network of AMMA (African Monsoon Multidisciplinary Analysis).

PM10 data from two stations of the "Sahelian Dust Transect"—M'Bour (Senegal; 16.96° W, 14.39° N) and Bambey (Senegal; 16.47° W, 14.70° N)—were utilized in this study. These measurement stations were deployed by the Interuniversity Laboratory of Atmospheric Systems (LISA) as part of the international research program AMMA. The objective of this program, particularly concerning desert aerosols, is to comprehensively document their variability and understand the controlling mechanisms [59].

PM10 concentrations were measured using Thermo Scientific's oscillating microbalances TEOM 1405 (April 2013 to July 2017) and TEOM 1400A (since November 2017) [60]. Data from the M'Bour station span from 2007 to 2019, while data from Bambey are available from 2014 to 2022, with hourly temporal resolution.

2.3.3. AERONET Data Set

AERONET (AErosol RObotic NETwork) is a network of ground-based sun photometers established in 1993 as part of NASA's Earth Observing System (EOS), in collaboration with the Centre National d'Études Spatiales (CNES) and the National Association of State Departments of Agriculture (NASDA). The global AERONET network includes over 500 stations. In West Africa, a French team from the Laboratoire d'Optique Atmosphérique (LOA) manages the AERONET/PHOTON component photometers, also known as CIMEL, which measure Aerosol Optical Depth (AOD) and the associated Ångström Exponent (AE). These instruments operate at various wavelengths, including 440, 675, 870, 940, and 1020 nm, with data recorded at 15-minute intervals [61].

The analyses conducted in this study rely on Level 2 data (highest quality), which have been interpolated to the 550 nm wavelength. This wavelength is considered representative of a "mean" AOD value from a spectral standpoint, as mentioned in [51]. The AE provides the spectral dependence of the measured AOD from visible to near-infrared wavelengths, giving insight into the sizes of aerosol particles; in particular, larger AE values correspond to larger particles.

Given $AE_{440–870}$ and assuming $AE_{550–870} \approx AE_{440–870}$, the AOD at 550 nm is determined using the following calculation:

$$AOD_{550} = AOD_{870} \times \left(\frac{550}{870}\right)^{AE_{440–870}}. \quad (2)$$

Daily AOD data from the Dakar station (Senegal; 16.959° W, 14.394° N) were used in this study, covering the period from 2003 to 2019.

2.3.4. CAMS Reanalysis

To study dust levels and atmospheric characteristics associated with HWs in Senegal, we utilized reanalysis data from the Copernicus Atmospheric Monitoring Service (CAMS). CAMS represents the fourth generation of global atmospheric composition reanalysis from the European Centre for Medium-Range Weather Forecasts (ECMWF). It provides a consistent data set for understanding long-term changes in global atmospheric composition and air quality. The CAMS reanalysis was generated using 4DVar data assimilation during ECMWF's Integrated Forecasting System (IFS) cycle 42r1 [62]. This system includes 60 hybrid sigma/pressure levels in the vertical dimension, with the

highest level at 0.1 hPa. Atmospheric data are available at these levels and are interpolated to 25 pressure levels, 10 potential temperature levels, and 1 potential vorticity level. Additionally, surface-level data are also provided (for more details, see the link: https://www.ecmwf.int/en/research/climate-reanalysis/cams-reanalysis, accessed on 14 March 2024). CAMS assimilates observational data, including AOD from MODIS (Moderate-Resolution Imaging Spectroradiometer) instruments on the Terra and Aqua satellites. The service provides estimates for several atmospheric parameters, including PM2.5, PM10, AOD at 550 nm, Dust AOD (AOD specifically related to dust particles), air temperature at 2 m (T2m), and the zonal and meridional components of wind at 925 hPa (denoted u and v, respectively). CAMS data have a temporal resolution of 3 h and a spatial resolution of 0.75° × 0.75°.

2.4. Statistical Methods

2.4.1. Validation Method

Validation involved comparing aerosol data from the CAMS reanalysis with various available observations to ensure the reliability and accuracy of CAMS data, particularly when applied to specific regions such as Senegal. Through comparing CAMS data with ground-based observations, we can assess how well the model represents local conditions, which is crucial for drawing meaningful conclusions. In our study, we used multiple observation data sets from different sites in Senegal to validate the CAMS reanalysis data. Observational data from the PurpleAir sensor network in Saint-Louis (2021–2022) were used to evaluate the performance of CAMS in representing the interannual variability and seasonal cycle of PM2.5 and PM10. PM10 concentrations from the INDAAF network were used to assess the accuracy of CAMS at the M'Bour (2007–2019) and Bambey (2014–2022) sites. Additionally, AOD data from the Dakar station (2003–2019) served as a reference for validating the CAMS data. The selection of these sites was based on the availability of relevant observational data for the aerosol parameters we studied.

2.4.2. Definition of Hot Day and Heat Wave

We adopted the definition proposed by Sambou et al. [52] to identify hot days and HW periods. A hot day is defined as a day when the maximum air temperature (Tx), minimum air temperature (Tn), or average apparent temperature (Ta) exceeds the corresponding moving 95th percentile threshold. This threshold is calculated over a 29-day window, ensuring a robust analysis through minimizing non-physical percentile fluctuations. The use of a moving detection threshold is essential, as our study focuses exclusively on the meteorological analysis of HWs and their associated mechanisms. This approach allows us to accurately capture the relevant synoptic signal while eliminating the influence of seasonal variations. An HW is defined as a series of at least three consecutive hot days.

2.4.3. Regionalization of Senegal

Our approach builds on recent studies that highlight the specific characteristics of HWs in Senegal, particularly in relation to the "regionalization method" proposed by Sambou et al. [52].

In this study, we employed hierarchical cluster analysis (HCA) to examine similarities in hot days across 12 meteorological stations from March to May, covering the period from 2003 to 2022. The HCA method progressively aggregates stations into clusters based on the simultaneous occurrence of hot days, with the Jaccard distance used to measure these similarities. To enhance the robustness of our analysis, we combined the HCA results for the Tx, Tn, and Ta variables. Further details on this regionalization method can be found in [52].

The dendrogram presented in Figure 3 illustrates the clustering of stations, indicating that Senegal can be divided into three homogeneous zones, each comprising four stations: Zone 1 (Saint-Louis, Dakar-Yoff, Ziguinchor, Cap Skirring) represents the coastal region, Zone 2 (Podor, Linguère, Diourbel, Kaolack) is classified as the intermediate zone, and

Zone 3 (Matam, Tambacounda, Kédougou, Kolda) corresponds to the inland region. These findings are consistent with those of [52], who regionalized daily heat extremes in Senegal.

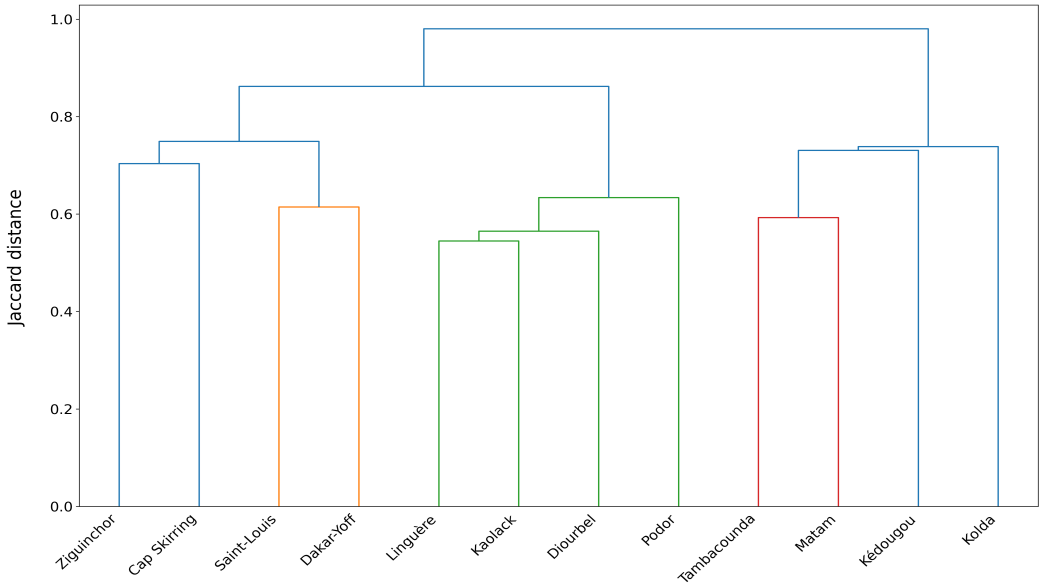

Figure 3. Combined hierarchical cluster analysis (HCA) for Tx, Tn, and Ta during spring (March–April–May) from 2003 to 2022. The dendrogram illustrates the appropriate number of clusters into which stations can be grouped.

2.4.4. Composite Analysis

In our study, we employed composite analysis to generate average aerosol concentration profiles during HW events. This method begins by grouping all the days associated with HWs. Next, we calculate composite anomalies for aerosol fields during these events, relative to the March–April–May (MAM) climatology. Finally, we compute time-shifted fields to better understand the aerosol distribution before, during, and after the onset of HWs.

2.4.5. Linear Regression and Statistical Significance

This study conducted linear regression analyses to quantify intra-seasonal atmospheric variability during the spring and to explore the links between atmospheric conditions and HWs in Senegal. Standardized temperature indices were calculated for each station and used as independent variables in the regressions. The anomalies of atmospheric parameters (Dust AOD, MSLP, u, v) were normalized, and linear regression was performed for each grid point (latitude, longitude):

$$Y = \beta_0 + \beta_1 X + \epsilon, \tag{3}$$

where Y is the anomaly of the parameter, X is the standardized temperature index, β_0 is the intercept, β_1 is the regression coefficient, and ϵ is the error term.

The statistical significance of the results was assessed using p-values, and only results with $p < 0.05$ were considered significant. The significant regression coefficients were visualized on maps.

2.4.6. Dust Exposure Assessment in Senegal

To assess exposure to fine particulate matter during the spring season from 2003 to 2022, we used daily PM2.5 and PM10 data from the CAMS reanalysis data set for Senegal. The air quality thresholds set by the Senegalese standard (NS 05-062, 2019)—which are 75 $\mu g/m^3$ for PM2.5 and 150 $\mu g/m^3$ for PM10—were applied. These thresholds are significantly higher than the WHO recommendations, which suggest limits of 25 $\mu g/m^3$

for PM2.5 and 50 μg/m^3 for PM10 [63]. For each grid point, days with PM2.5 and PM10 concentrations exceeding these thresholds were classified as "unhealthy days". The percentage of unhealthy days for each grid point was calculated by dividing the number of unhealthy days by the total number of days in the spring and then multiplying the result by 100. These percentages were spatially interpolated to generate continuous maps illustrating the spatial distribution of PM exposure across Senegal.

3. Results

3.1. Validation of CAMS Products

Figure 4a compares the inter-annual variability in PM2.5 concentrations from CAMS with measurements from 11 sites in Saint-Louis. The CAMS data consistently overestimated PM2.5 concentrations throughout the entire study period. However, both the observations and CAMS data exhibited a strong visual alignment, with peaks and troughs closely corresponding to one another. Notably, PM2.5 values recorded at the Pikine and Bango stations exhibited a different trend when compared to the other stations. This discrepancy suggests that these two sites may be influenced by specific pollution sources not affecting the other locations, potentially due to unique local conditions.

The performance of CAMS data in reproducing the seasonal cycle of PM2.5 concentrations in Saint-Louis is shown in Figure 4b. Higher PM2.5 levels are observed during the dry season, while lower levels are observed during the rainy season. Despite consistent overestimation, the CAMS data effectively captured the global pattern.

The PM10 time-series presented in Figure 4c,d show trends similar to those observed in Figure 4a,b, with higher PM10 concentration levels.

Figure 4e–h compare PM10 concentration data from CAMS reanalyses and observations at Bambey and M'Bour. The results show a much more satisfactory match between CAMS data and observations regarding interannual variability (Figure 4e,g); however, the CAMS reanalysis considerably underestimated PM10 levels for both Bambey and M'Bour.

Analysis of the PM10 seasonal cycle (Figure 4f,h) indicated that concentrations peak during the dry season and reach their lowest levels in the rainy season. These results are in line with the works of [59,64]. According to these authors, PM10 concentrations reach a maximum around March and a minimum in August. Evaluation of CAMS products across the seasonal cycle indicated a fairly accurate reproduction of PM10 maxima and minima at both M'Bour and Bambey. PM10 trends during the rainy season (June to September) were captured well by CAMS, with values closely matching the observations. However, during the dry season, when PM10 concentrations are higher, a significant discrepancy between CAMS and observations was observed, particularly from December to February. This discrepancy was more pronounced for M'Bour than for Bambey.

As seen for the representation of interannual variability, CAMS underestimated PM10 concentrations during the dry season (October to May) at both stations. However, CAMS overestimated PM10 levels in August and September for Bambey. The correlations calculated for the monthly time-series were 0.92 for Bambey and 0.87 for M'Bour, indicating a strong correlation between CAMS data at both the continental (Bambey) and coastal (M'Bour) stations.

Figure 4i illustrates the interannual variability in AOD for Dakar, comparing CAMS data with AERONET observations. The CAMS and AERONET data exhibited similar variability over the years, with peaks and troughs in both series often aligning, indicating interannual consistency between the two data sets. However, CAMS generally overestimated AOD fluctuations.

Figure 4j shows the seasonal climatology of AOD from CAMS compared with the AERONET in situ measurements for Dakar. The results reveal that CAMS accurately reproduced the peaks and troughs of AOD between January and December, with a peak in June. Nevertheless, CAMS considerably overestimated the annual AOD cycle, particularly between March and October. The monthly AOD averages at the Dakar station align with findings of studies by [65,66], who also reported similar seasonal characteristics.

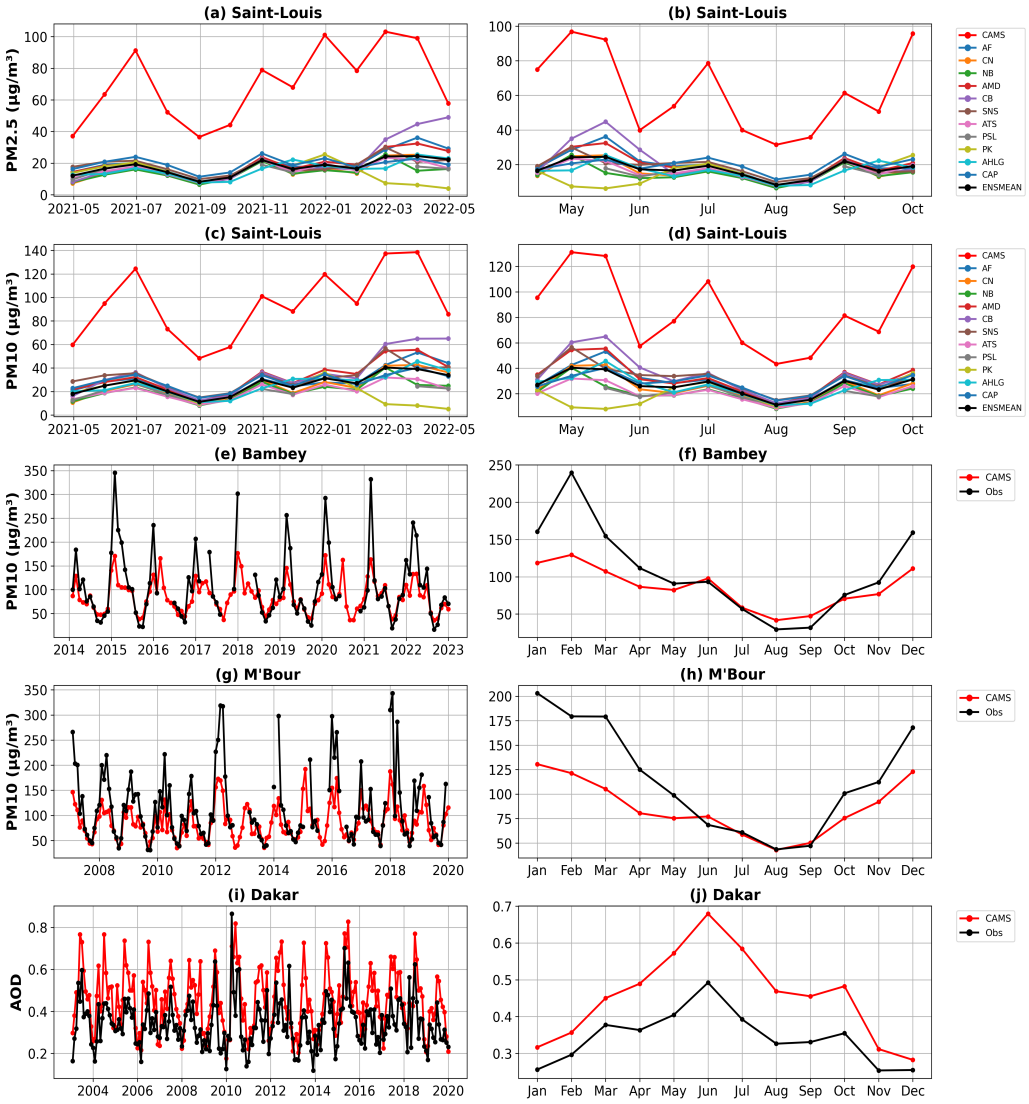

Figure 4. Comparison of PM2.5 and PM10 concentrations (µg/m^3) between CAMS (represented by the red curve) and PurpleAir observations (shown in different colors, with Ensemble Mean ENSMEAN in black) in Saint-Louis (**a**–**d**); CAMS PM10 with INDAAF observations (Obs) in Bambey and M'Bour (**e**–**h**); and CAMS AOD with AERONET observations in Dakar (**i**,**j**).

We observed a phase opposition between the seasonal cycles of AOD and PM. These findings are consistent with previous studies by [47,67]. The divergence between these two parameters can be attributed to the vertical distribution of dust: the Saharan Air Layer (SAL) frequently transports dust at higher altitudes, while lower levels may show reduced PM concentrations [68]. When the SAL is elevated, dust remains aloft and does not significantly contribute to surface PM levels, resulting in a dissociation between AOD and PM. In contrast, when the SAL descends, surface dust concentrations increase, leading to higher PM levels.

Validation of aerosol data from the CAMS reanalysis demonstrated a good agreement with the PM2.5, PM10, and AOD observations from PurpleAir, INDAAF, and AERONET, respectively (Figure 4). However, the CAMS reanalysis significantly overestimated PM2.5 and PM10 concentrations at the 11 PurpleAir sensor stations in Saint-Louis (Figure 4a–d). This overestimation is likely due to the relatively coarse resolution of the CAMS data ($0.75^\circ \times 0.75^\circ$). Recent advances in dust models have improved the representation of dust distribution patterns in West Africa, primarily due to enhanced parameterization of land surface conditions [16]. Nonetheless, evaluating dust content using surface measurements

in West Africa remains challenging due to the scarcity of continuous data and limited spatial coverage. Despite these challenges, CAMS successfully captures the temporal variability at specific locations in Senegal, such as Saint-Louis, where dust measurement networks are established. Several studies have assessed the performance of CAMS in representing atmospheric aerosol loads. For instance, the CAMS hourly PM2.5 data have been validated against ground-based measurements in the USA and China [69,70], which revealed that CAMS overestimated PM levels during clean, moderately polluted, and highly polluted days across China. The discrepancies observed in these studies are likely due to uncertainties in the vertical distribution of aerosols, aerosol composition, mass extinction efficiency, and the size distributions of dust and sea-salt particles, as well as the differences between aerodynamic and geometric sizes. Ukhov et al. [71] found that the overestimation of CAMS PM2.5 over the Middle East and West Asia could be linked to poor size distribution data for emitted dust. Similarly, Royé et al. [72] compared CAMS and observed PM concentrations from field monitoring stations in 33 provincial capitals in Spain and observed an underestimation of reanalysis data and a substantial discrepancy in the shapes of the concentration distributions. Our findings in Senegal align more closely with those from studies in China [69] and the Middle East and West Asia [71]. In Morocco, Sekmoudi et al. [73] validated PM10 data from the CAMS reanalysis by comparing them with daily average PM10 concentrations recorded at six air quality monitoring stations during 2016. Their results revealed a strong seasonal dependency, with a positive bias in winter and a negative bias in summer. Asutosh et al. [32] studied a Saharan dust storm event from 14 to 19 June 2020, and showed that the CAMS reanalysis successfully captured this event's AOD. However, the AOD values from CAMS were slightly underestimated when compared with MODIS and OMI (Ozone Monitoring Instrument) satellite products. Overall, CAMS data have proven valuable for climate studies, particularly in analyzing seasonal, extreme, and annual variations in PM10 concentrations. Pakszys et al. [74] demonstrated that the CAMS model effectively reproduced aerosol temporal variability and the dominant aerosol types at the Kongsfjorden and Hornsund stations between 2010 and 2015.

3.2. Characterization of Aerosols Associated with Heat Waves

3.2.1. Mean Seasonal Variation

Figure 5 shows the variation in the monthly average PM2.5 concentrations from 2003 to 2022, highlighting the decreasing values at synoptic stations in Senegal in relation to Tx, Tn, and Ta.

The results indicate that the continental stations exhibit an annual temperature distribution with two peaks in Tx: a main peak in the spring (March–April–May) and a secondary, weaker peak in the fall (October–November). Coastal stations (Dakar-Yoff, Saint-Louis, and Cap Skirring) present a different temperature pattern. At Dakar-Yoff, maximum temperatures are particularly high between May and November, with a peak recorded in October. In the Sahel (e.g., Bamako and Niamey), both southwesterly and northeasterly winds occur with roughly equal annual frequency [75–77]. However, Dakar-Yoff is an exception, with northerly winds dominating. On the west coast, the Intertropical Convergence Zone (ITCZ) curves towards the equator, and Dakar-Yoff is rarely located on its equatorial flank. As a result, Dakar-Yoff is influenced by the North Atlantic trade wind system throughout the year. At Saint-Louis and Cap Skirring, a first peak in Tx occurs in March, followed by a second peak in November. For the continental stations in Senegal, Tx values are generally low between December and February, then increase rapidly between March and May. The onset of the rainy season leads to a drop in temperatures, which rise again after the rainy season ends.

Regarding minimum temperatures, continental stations such as Kédougou, Tambacounda, and Matam exhibit a bimodal cycle, with a more significant first peak between April and May than the second peak recorded in October. The bimodal cycle of Tn is less pronounced at other continental stations. The first peak occurs in May for Kolda and Podor,

and slightly later in the year (between June and July) for the other stations. The second peak is observed in October across all continental stations. In contrast, coastal stations present a unimodal cycle, with maximum values recorded between June and October.

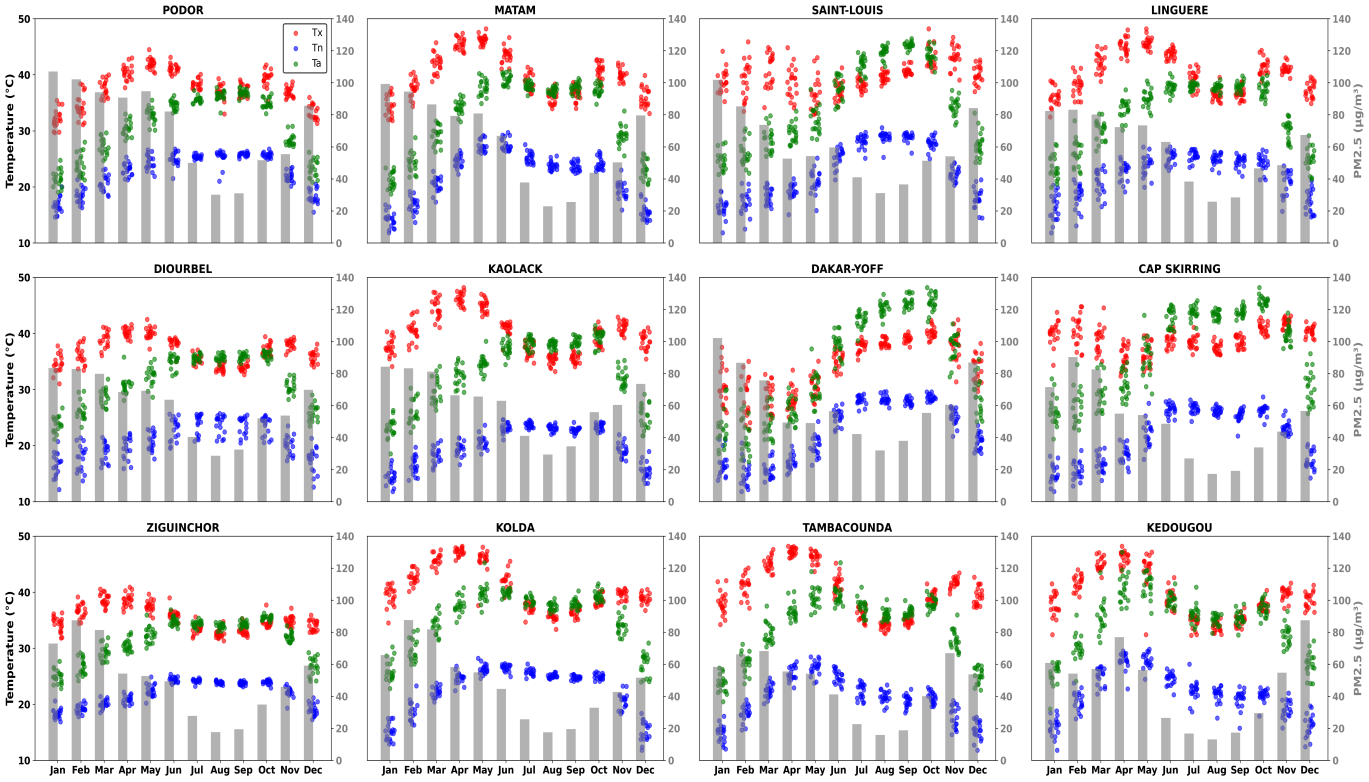

Figure 5. Seasonal cycles of PM2.5 (gray bars) and temperatures (Tx in red, Tn in blue, Ta in green) across 12 stations in Senegal. Stations are arranged (from left to right, top to bottom) by decreasing dust concentrations.

The seasonal variation in Ta can be interpreted as a combination of temperature and humidity, which results in its peak shifting to the summer months, even at continental stations.

The seasonal cycle of PM2.5 concentrations shows that maxima occur during the dry season and minima during the rainy season, with peaks recorded in January and February. In contrast, Dust AOD reaches its maximum slightly later, between March and June (see Figure S1).

Northern stations, such as Podor, Linguère, and Matam, experience higher temperatures and elevated PM2.5 levels, reflecting their arid conditions and frequent dust episodes. Central stations such as Kaolack and Diourbel exhibit similar trends to the arid stations, with high temperatures but moderate PM2.5 levels. The Dakar-Yoff and Cap Skirring stations, influenced by maritime conditions, show more moderate temperatures and less pronounced seasonal variations, although PM2.5 peaks are still evident early in the year. Southern stations, such as Tambacounda and Kédougou, present lower PM2.5 concentrations.

The difference in the timing of the peaks between PM2.5 and Dust AOD can be explained by the distinct origins of these particles. Dust AOD is primarily influenced by desert dust lifting events, which occur under the influence of Harmattan winds, typically being more active at the beginning and end of the dry season. In contrast, PM2.5 is largely a result of anthropogenic sources, such as biomass burning, bushfires, and urban activities, which tend to increase in January and February, when drought conditions are more pronounced and local accumulation of fine particles is favored. The simultaneous minimum levels observed during the rainy season for both types of particles can be attributed to the atmospheric washing effect caused by rainfall, which significantly reduces airborne particle concentrations. Regarding PM10, as presented in the Supplementary Materials

(Figure S2), a trend similar to that of PM2.5 is observed, with maximum concentrations during the dry season. These results are consistent with previous studies indicating that fine particulate levels are highest during the dry season and lowest during the rainy season, due to both local and regional pollution sources as well as natural contributions, such as Saharan dust [47,59,64].

Spring marks the first temperature peak at most stations in Senegal, and is also a period characterized by increased dust loads. Given this, we chose to focus our study on this season, as it is the hottest in Senegal and is characterized by frequent dust episodes. Although PM2.5 and PM10 concentrations tend to peak earlier in the year—mainly in January and February—including PM in our analysis remains essential, as its impact on air quality extends into spring. According to Diokhane et al. [37], large-sized particles negatively impact air quality and upper respiratory health, primarily during the winter and spring seasons. AOD is a key optical parameter for evaluating aerosol content in the atmosphere and assessing air pollution. Many studies have also used this parameter in conjunction with PM to explore the links between dust levels and health impacts in Africa [37,47,78]. In this context, we have also used it alongside PM to further investigate the effects of dust on HWs.

Figure 6 shows the mean air temperature fields at 2 m (T2m), sea level pressure (MSLP), wind at 925 hPa, fine particle concentrations (PM2.5 and PM10), Aerosol Optical Depth (AOD), and Dust AOD (AOD specifically related to dust particles) for the March–April–May (MAM) season from 2003 to 2022. Maximum temperature values are observed over the continent between 10° N and 20° N, with surface pressure values around 1010 hPa. Higher pressures are recorded over the ocean (around 1020 hPa), centered around 30° N (Figure 6a). The strong zonal pressure gradient between the Saharan Thermal Low over the continent and the Azores High over the ocean generates winds flowing from high-pressure areas to low-pressure areas (Figure 6b). These north/northeasterly trade winds travel along the Senegalese coast, with part of the airflow crossing the continent from Western Sahara and Morocco, reaching mainland Senegal through the desert region of Mauritania. Winds are most intense at ocean level, reaching a maximum of 8 m/s between 10° N and 20° N. The convergence between the moisture-laden southeasterly trade winds and the northerly trade winds marks the Intertropical Convergence Zone (ITCZ), where wind speeds are minimal.

Figure 6c–f show the climatology of PM10, PM2.5, AOD, and Dust AOD for the MAM season from 2003 to 2022, respectively. Although these four measurements are related to atmospheric aerosols, they differ in terms of the nature of the particles they represent and their measurement methods.

The climatology of PM10 and PM2.5 concentrations is illustrated in Figure 6c and Figure 6d, respectively. PM10 comprises coarse particles, including desert dust, volcanic ash, and particles from anthropogenic sources such as industrial emissions and vehicle exhaust. PM2.5 consists of finer particles primarily deriving from human activities, such as biomass combustion and vehicle emissions, as well as secondary particles formed in the atmosphere. The results indicate high PM10 and PM2.5 concentrations north of 10° N on the continent. PM10 concentrations are generally higher as they encompass both PM2.5 particles and larger coarse particles. The areas with the highest values include Western Sahara, northern Algeria, and the border region between Mali and Mauritania, as well as parts of Libya, Chad, and Guinea.

The climatology of AOD during the spring season is illustrated in Figure 6e. AOD measures the extinction of light by particles suspended in a vertical column of air. It serves as an indicator of the total concentration of aerosols in the atmosphere, as well as their ability to absorb and scatter light. AOD encompasses both fine and coarse particles from various sources (both natural and anthropogenic). The results reveal a strong AOD signal south of 20° N on the continent, with maximum values observed in Guinea, Sierra Leone, and Nigeria. This is partly attributed to frequent biomass burning in these regions. In the ocean, a distinct AOD signal is also observed due to aerosol transport by winds from the major source areas. Figure 6f presents the mean climatology of Dust AOD during spring.

Dust AOD indicates the concentration of mineral particles in the atmosphere, which is a major component of PM10 and, to a lesser extent, PM2.5. A strong Dust AOD signal is observed between 10° N and 20° N, where mineral aerosol sources are particularly active. The northward migration of the ITCZ, coupled with the rise of the Saharan Thermal Low, favors the intense dust signal observed in the northern parts of Africa.

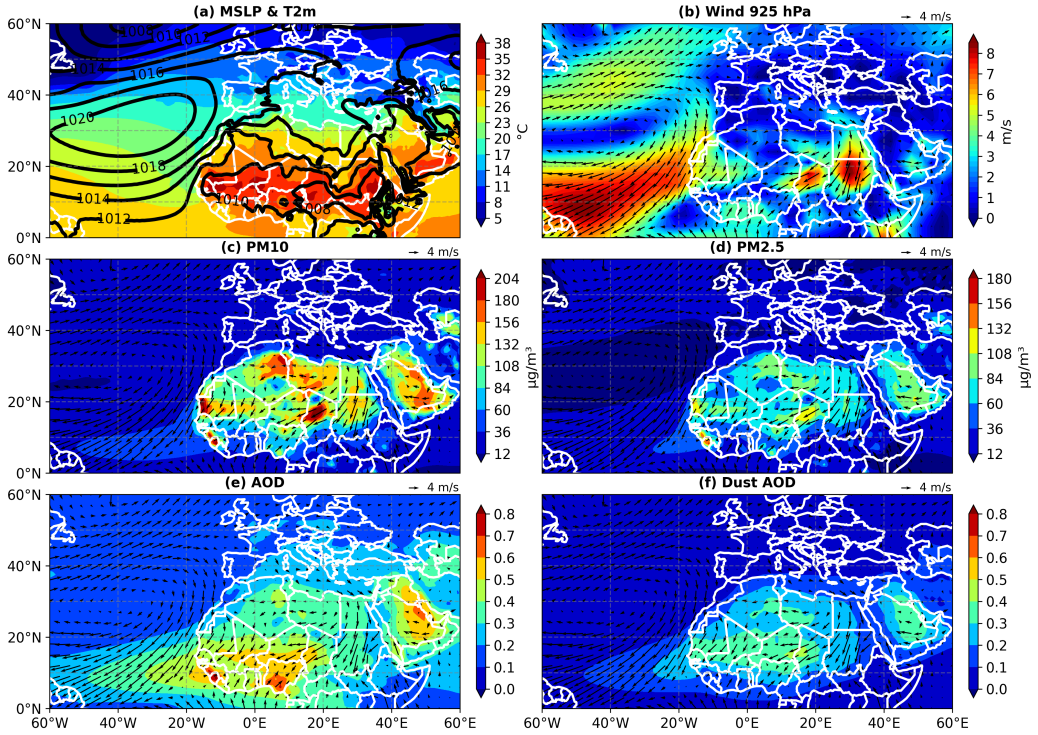

Figure 6. Climatology of MSLP (contours) and T2m (colors) fields from CAMS for March–April–May over the period 2003–2022 (**a**); wind speed at 925 hPa is shown in color and direction in arrows (**b**); the climatology of PM10, PM2.5, AOD, and Dust AOD fields (contours) and wind direction (in arrows) for the same period and season are shown in (**c**), (**d**), (**e**), and (**f**), respectively.

In addition to the spatial distribution, dust layers exhibit seasonal vertical variations. Previous studies have shown that dust layers transported away from their sources are generally elevated to higher altitudes when compared to dust near its origin. The altitude of dust layers varies seasonally. Over the West African continent, dust layers are situated at lower levels (near the surface) during the winter, while during the summer they are elevated to higher altitudes [79]. This seasonal variation is driven by the main features of the West African monsoon. In the summer, the northward shift of the Intertropical Discontinuity (ITD) and increased solar radiation lead to enhanced surface heating. As a result, the boundary layer becomes deeper, promoting stronger upward mixing of dust [80,81]. Additionally, dust layers in the mid-troposphere, which overlay the humid and denser monsoon air, reach higher transport levels in the summer compared to winter, when the dust is typically confined to lower levels within the trade winds [79]. In winter, as noted previously [80], the dust transport layer is situated at lower tropospheric levels, with maximum dust concentrations generally up to around 2 km on most days, and frequently extending to near-surface levels. In spring, the dust transport layer is typically found at lower tropospheric levels (up to about 2 km), but can also extend to higher altitudes (around 4 km). During the summer, the dust transport layer becomes part of the Saharan Air Layer (SAL), which is situated around 4–5 km above the surface and does not extend to near-surface levels. This seasonal vertical layering of the dust cycle over the Sahel region has also been described by [82].

3.2.2. Regionalization of Heat Waves and Associated Aerosol Patterns over Senegal

Figure 7 presents a detailed analysis of HWs detected with respect to different temperature measurements: Tx-HW for HWs detected with maximum air temperature (Tx), Tn-HW for those detected using minimum air temperature (Tn), and Ta-HW for HWs detected using average apparent temperature (Ta) across all of Senegal. The results show that the maximum duration of Tx-HW is 8 days (Figure 7a), 10 days for Tn-HW (Figure 7b), and 12 days for Ta-HW (Figure 7c).

The average duration was similar for all three types of heat waves (i.e., Tx-HW, Tn-HW, and Ta-HW), each being around 4 days. In terms of the number of events, Ta-HW recorded the highest frequency (83 events), followed by Tx-HW (66 events) and Tn-HW (47 events). The results also indicate that simultaneous HWs across several stations are rare. Grouping stations based on their similarity in terms of hot days does not necessarily mean that HWs occur at the same times across these stations. Several factors can explain the observed discrepancies in HW occurrences between stations within the same climatic region. Intra-seasonal variability during the spring season can lead to local atmospheric fluctuations, causing HWs to occur at different times despite similar climates. Additionally, factors such as vegetation, soil moisture, and proximity to bodies of water can modulate temperatures and shift the onset of HWs. Tx-HW events appear to be more frequent from 2012 onwards, particularly at the stations of Matam, Linguère, Kédougou, Kaolack, Kolda, and Diourbel. Regarding Tn-HW, these stations recorded few events between 2017 and 2022 and, similarly, Ta-HW events were sparse between 2019 and 2022. No clear trend towards an increase in HW duration was observed between 2003 and 2022 for any of the three HW types.

Figure S3, presented in the Supplementary Materials, illustrates the distinct characteristics of HWs across the three zones of Senegal (Zone 1, Zone 2, and Zone 3). This analysis highlights the differences in HW frequency and duration. For Tx-HW, the most common events lasted between 3 and 5 days in all zones. Although simultaneous HW occurrences across stations have been recorded, it is rare to observe them happening concurrently at all three stations. For instance, the HW events of 9 March 2013 and 20 April 2016 in Zone 2 affected three stations, each with an average duration of 4 days. Zone 3 has witnessed an increase in HW frequency since 2010, unlike Zones 1 and 2, which exhibited more interannual variability. However, no significant trend toward an increasing HW duration is observed. In Zone 1, the stations of Saint-Louis and Dakar-Yoff experienced the highest number of HW events, while the southern stations of Ziguinchor and Cap Skirring had fewer occurrences. In Zone 2, Podor and Diourbel registered more events compared to Kaolack and Linguère. In Zone 3, HW events were more evenly distributed across the stations. Overall, Zones 1 and 2 recorded more Tx-HW events (32 and 24, respectively) than Zone 3 (10 events). The results also showed that Tn-HW events, lasting between 3 and 5 days, were common, similar to Tx-HW. A notable event in Zone 1 occurred on 26 May 2005, affecting Dakar-Yoff, Cap Skirring, and Saint-Louis, with an average duration of 4 days. Several other HW events occurred simultaneously, particularly in 2005 and 2012. Across all zones, Ta-HW events tended to last longer than both Tx-HW and Tn-HW, with an average duration of 6 days. Zone 1 registered the highest number of Ta-HW events (31), followed by Zone 3 (27) and Zone 2 (25). Notably, Zone 3 experienced more Ta-HW events (27) than Tx-HW (10) and Tn-HW (13). Table 1 summarizes the number of HW events detected across the three zones of Senegal.

Table 1. The number of Tx-HW, Tn-HW, and Ta-HW events detected across the three zones from 2003 to 2022.

Zone	Tx-HW	Tn-HW	Ta-HW
Zone 1	32	22	31
Zone 2	24	12	25
Zone 3	10	13	27

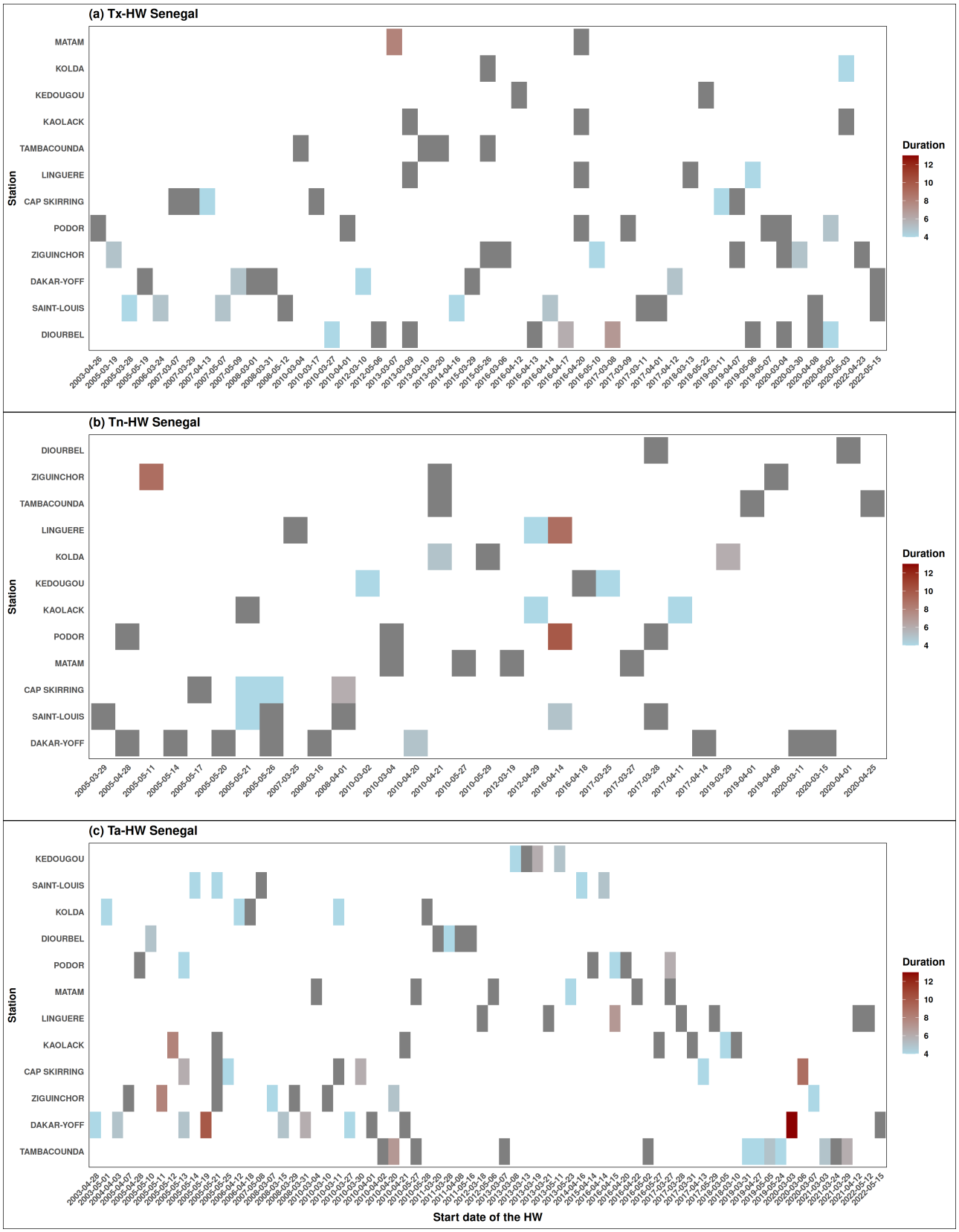

Figure 7. Evolution of Tx-HW (**a**), Tn-HW (**b**), and Ta-HW (**c**) in Senegal between 2003 and 2022. The horizontal axis shows the start dates of each HW, while the vertical axis represents the different synoptic stations. The color of each bar reflects the duration of the HW in days, with darker shades of red indicating longer periods and lighter shades of blue indicating shorter events.

The study of HW evolution across the three defined zones revealed notable disparities. Zone 1 recorded the highest number of HW episodes. Our results align with the findings of Sambou et al. [52], who examined the occurrence of spring HWs in Senegal from 1979 to 2014. Their analysis indicated that Zone 1 experienced the highest number of Tx-HW events, with 41 occurrences, compared to Zones 2 and 3, which recorded 29 and 18 events, respectively. Similarly, Zones 1 and 2 experienced more Tn-HW than Zone 3, with 31, 36, and 20 events, respectively. For Ta-HW, Zone 1 again stood out with 41 events, while Zone 2 recorded 34 and Zone 3 recorded 37. The fact that Zone 1 recorded the highest number of HW events can be partly explained by the low percentage of missing data at the stations in Dakar-Yoff, Saint-Louis, Ziguinchor, and Cap Skirring, which make up this zone. Although missing data in temperature series were initially filled using the MissForest method, the high percentage of missing data in certain stations in Zones 2 and 3—such as Diourbel and Kédougou (see Figure 1)—made the MissForest method less effective. Moreover, when missing values are distributed successively over a long period, the imputation method has limitations [57].

To illustrate the modulation of HWs detected in Senegal (across all zones) by different types of aerosols, we present composite maps. Figure 8 displays a composite analysis of PM2.5, PM10, AOD, and Dust AOD concentrations in Senegal, based on all HW days detected using Tx, Tn, and Ta.

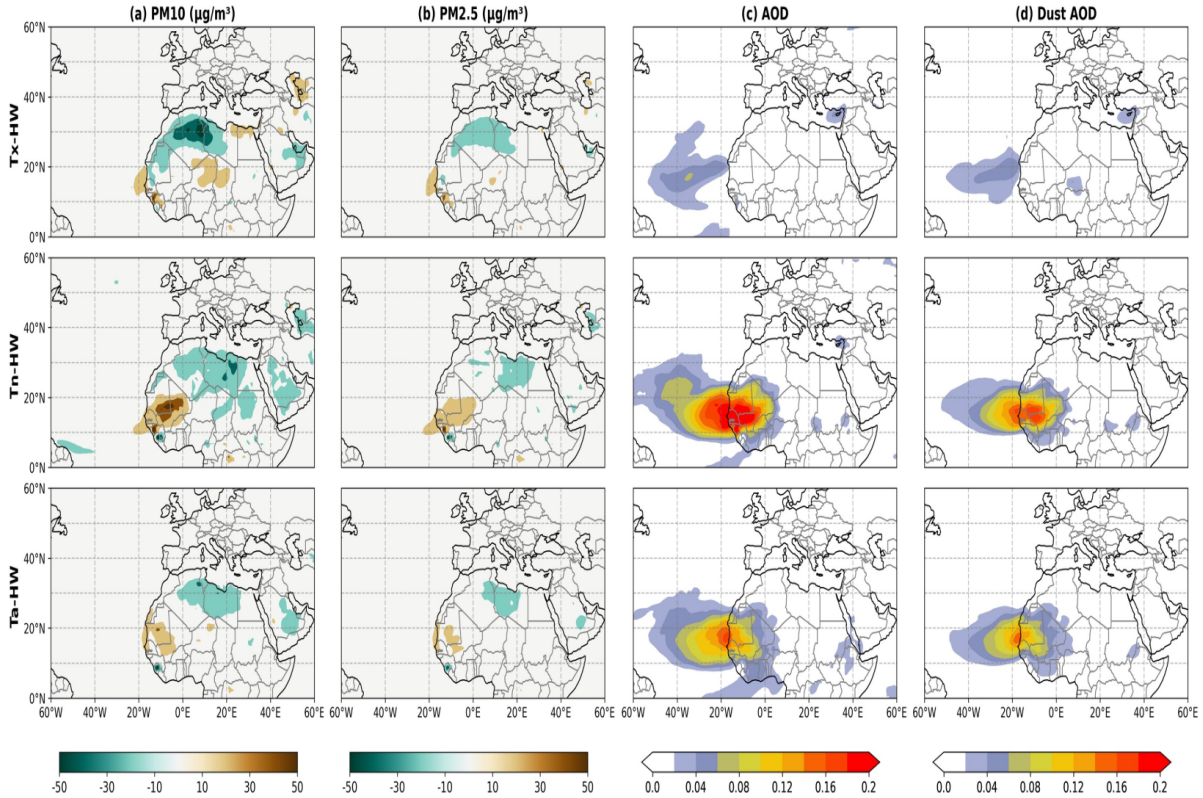

Figure 8. (**a**) Composite of deseasonalized anomalies of PM10 (µg/m^3) concentrations, (**b**) PM2.5 (µg/m^3) concentrations, (**c**) AOD, and (**d**) Dust AOD during Tx-HW (1st row), Tn-HW (2nd row), and Ta-HW (3rd row) in Senegal from 2003 to 2022.

The PM10 composites for Tx-HWs, Tn-HWs, and Ta-HWs are shown in Figure 8a. The results reveal a positive PM10 anomaly over the coastal part of Senegal, with a negative anomaly extending towards Algeria and Libya, slightly reaching northern Mauritania for Tx-HWs. For Tn-HWs, the PM10 composites show a negative anomaly centered towards Libya, while a positive anomaly covers the entire Senegalese territory. In the case of Ta-HWs, the PM10 anomaly is negative over parts of Algeria and Libya, with a positive anomaly over northwestern Senegal, as well as parts of Mali and Mauritania.

The differences between PM10 and PM2.5 composites (Figure 8b) are primarily related to the spatial distribution of anomalies; in particular, the distinction between positive and negative anomalies is more pronounced for PM2.5. Negative anomalies towards Algeria are more prominent for PM10, with a tendency to infiltrate northern Senegal for both Tx-HWs and Tn-HWs. A positive anomaly is also observed in Chad and Sudan during Tn-HWs.

Figure 8c shows the presence of a positive AOD anomaly over the ocean, but not touching Senegal for Tx-HWs. This suggests that Tx-HWs in Senegal are not always associated with high aerosol concentrations. However, for Tn-HWs and Ta-HWs, a strong AOD signal covers all of Senegal and extends to the ocean. These findings indicate that Tn-HW and Ta-HW events in Senegal are linked to significant aerosol loads, especially in northwestern Senegal and along the Senegal–Mauritania border.

The Dust AOD composites presented in Figure 8d show patterns similar to the AOD composites for both the Tn-HW and Ta-HW. Positive anomalies are located in approximately the same positions, but with lower intensities and a more limited spatial extent for Dust AOD. The results highlight that Tn-HWs and Ta-HWs in Senegal are linked to the presence of large aerosol concentrations extending into the Saharan region, particularly over the entire Senegalese territory. In contrast, Tx-HWs coincide with aerosol loads that primarily extend over the extreme western part of Senegal, particularly along the Senegal–Mauritania coast.

Given that the composites for PM2.5, PM10, AOD, and Dust AOD exhibited similar spatial patterns (see Figures S4–S6), we focus on presenting the results of the Dust AOD composites for the three zones of Senegal.

Figure 9 compares Dust AOD anomalies during Tx-HW, Tn-HW, and Ta-HW events across Zones 1, 2, and 3. The results indicate that HW events in Zone 1 are associated with dust anomalies covering a large area, including parts of the Atlantic Ocean and West Africa. In Zone 2, Dust AOD composites for Tx-HWs, Tn-HWs, and Ta-HWs show that Tx-HWs are not associated with high dust concentrations, unlike Tn-HWs and Ta-HWs. A similar pattern can be observed in Zone 3, where Tx-HWs are not linked to positive Dust AOD anomalies, while Tn-HWs and Ta-HWs show such associations.

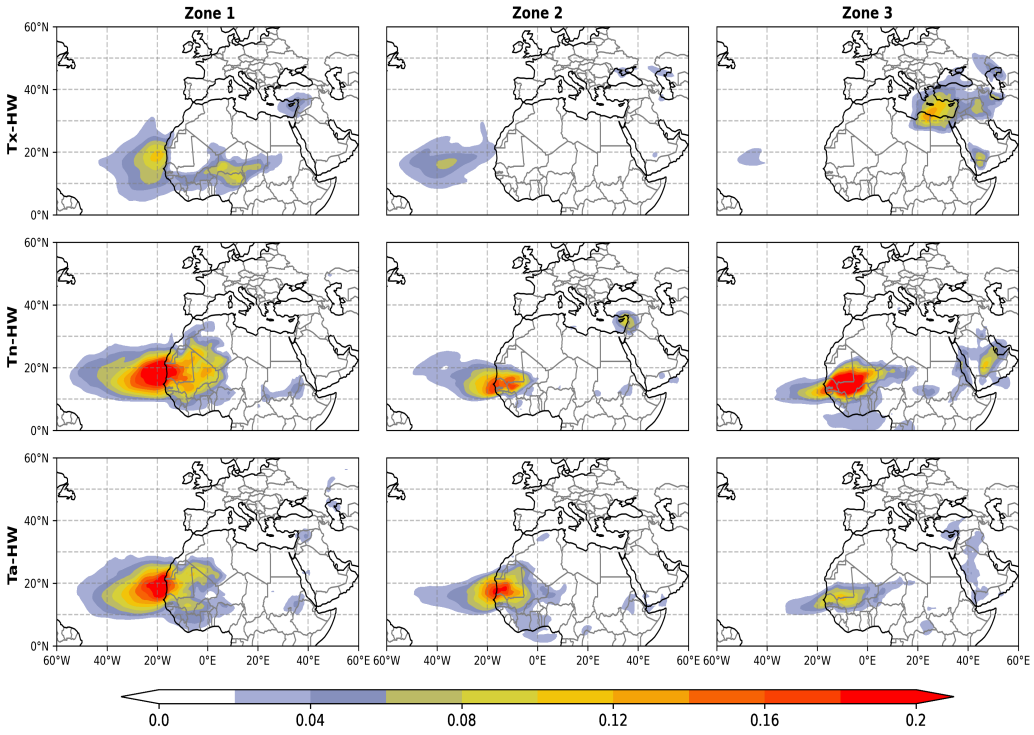

Figure 9. Composite of deseasonalized anomalies of Dust AOD for Tx-HW (1st row), Tn-HW (2nd row), and Ta-HW (3rd row) in Zone 1 (1st column), Zone 2 (2nd column), and Zone 3 (3rd column) of Senegal.

A comparison of Tx-HW composites between the three zones revealed a positive dust anomaly over the 10° N–20° N band, covering most of Senegal. However, in Zones 2 and 3, Tx-HW composites do not show the presence of a positive anomaly over Senegal, suggesting that Tx-HWs in these zones are not necessarily linked to dust events. For Tn-HWs, composites from Zones 1, 2, and 3 revealed a positive anomaly that extends over much of West Africa, including Senegal. This indicates that Tn-HWs in all three zones are associated with significant desert aerosol loads. Finally, the Ta-HW composites demonstrated a positive anomaly over Senegal, with varying intensity across the zones. Zones 1 and 2 are associated with higher concentrations of desert dust, while Zone 3 shows a lower intensity.

To determine which zone contributes most to the strong aerosol signal during Tx-HWs, Tn-HWs, and Ta-HWs, we compared Figures 8 and 9. The results indicate that the strong signal observed over the ocean and near the Senegalese coast during Tx-HWs is largely due to contributions from Zones 1 and 2, with Zone 1 being the primary contributor. For Tn-HWs, all zones contribute to the presence of dust in Senegal, although to varying degrees: Zone 1 contributes the most, followed by Zone 2, and then Zone 3. Similarly, for Ta-HWs, Zone 1 contributes the most, followed by Zones 2 and 3.

3.3. Dusty Heat Waves and Associated Synoptic Patterns

3.3.1. Composite Circulation Anomalies Associated with Heat Waves

To understand the mechanisms involved in the modulation of HWs by dust across the three zones of Senegal, we plotted time-lagged composites starting four days before the onset of the HWs and extending to four days after their onset.

Figure 10 illustrates the temporal evolution of composite Dust AOD, MSLP, and wind anomalies at 925 hPa, focusing on the periods before, during, and after the start of Tx-HW events (T0) in Zones 1, 2, and 3.

Analysis of the Zone 1 results reveals a positive dust anomaly over a large portion of the ocean between 5° N and 20° N at Lag −4. This positive dust anomaly intensifies at Lag −2, with a pronounced signal extending towards the Mauritanian coast. At Lag 0, the dust signal weakens, showing reduced spatial extent towards the Mauritanian coast, and disappears completely by Lags 2 and 4. This variation in dust distribution is linked to the weakening of the Azores anticyclone, which drops by approximately 3 hPa at Lag −4, favoring the upwelling of southeasterly winds and, consequently, the northward movement of dust at Lag −2. Additionally, a positive pressure anomaly of around +3 hPa is observed over Europe at Lag −4. This MSLP anomaly progressively shifts towards Africa, reaching as far as Algeria by Lag 0, generating northerly winds that transport the dust towards Senegal. Two days after the start of the HW event, the positive pressure anomaly towards Algeria gradually weakens, and the Azores anticyclone begins to strengthen, causing the dust to dissipate. Similar patterns can be observed in the lagged composites for fine particles (see Figures S7 and S8).

The results for Zone 2 Tx-HW indicate no positive dust anomalies over Senegal at Lags −4 and −2. At Lag 0, a positive dust anomaly appears near the Senegalese coast; however, it dissipates completely two days later. In Zone 3, the lagged composites indicated no Dust AOD signal over Senegal or the surrounding regions, either four days before, during, or four days after the onset of Tx-HW. These findings are consistent with those of Sambou et al. [52], who demonstrated that positive pressure anomalies centered around the Strait of Gibraltar can promote east-to-northeast wind anomalies which, in turn, lead to higher temperatures in Senegal. The primary synoptic patterns associated with the Sahel Dust Zone (located between 10° N and 16° N) involve the extension of the Azores High into Northwest Africa, accompanied by a cyclone over Northeast Africa. To the east of North Africa (around 15° E), a low-pressure system centered over Libya and Egypt dominates, while the western part of North Africa is influenced by the Azores High. This atmospheric configuration produces a northerly flow over central North Africa, which then turns towards the monsoon trough, typically located around 10° N in early spring [83]. In this setup, dust lifted from source

regions in Libya, Chad, Mali, Niger, Morocco, and Mauritania and is transported toward the convergence zone over the southern Sahel, resulting in suspended dust in that region [84].

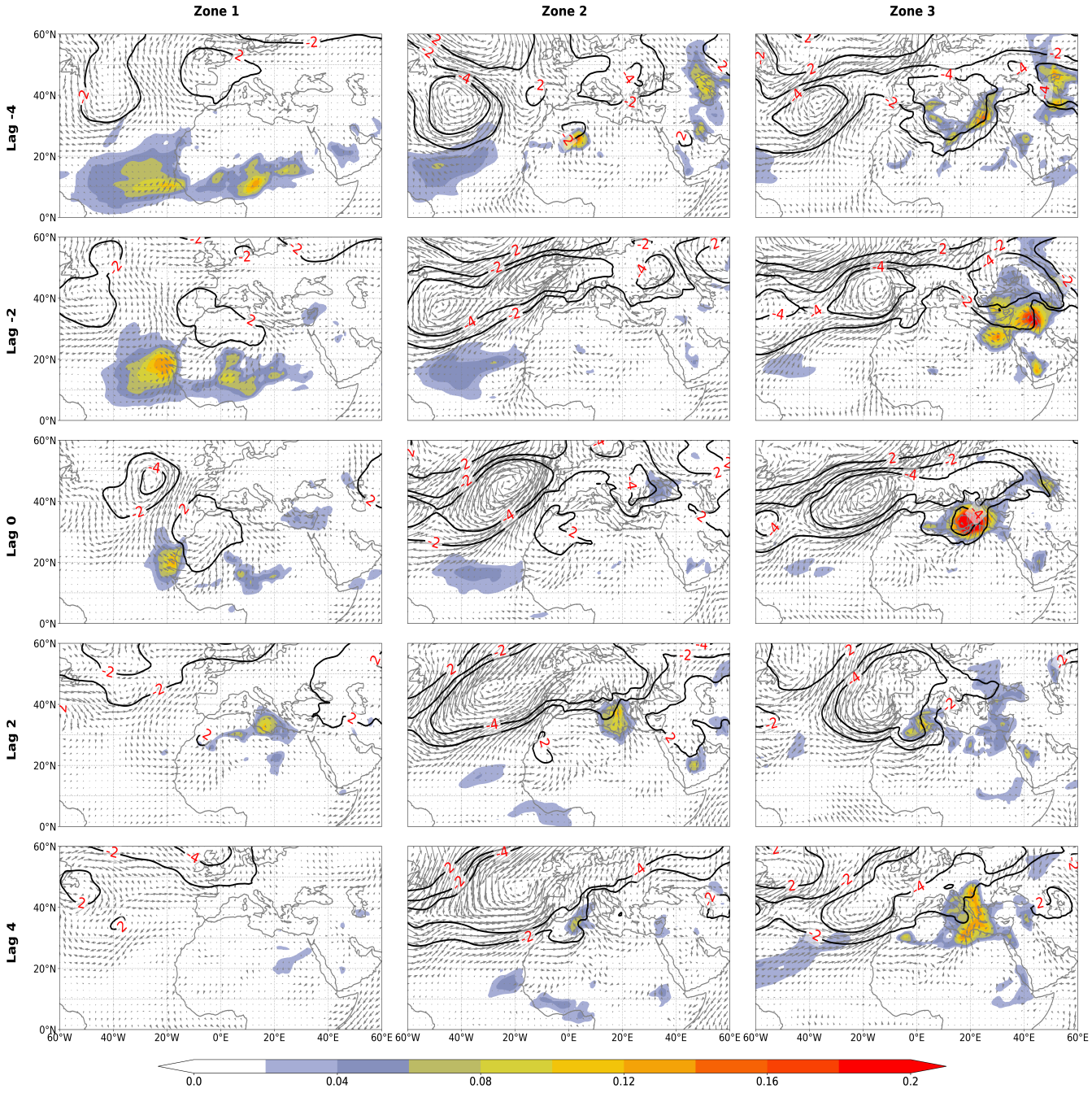

Figure 10. Composite of deseasonalized anomalies of Dust AOD during Tx-HW for Zone 1 (1st column), Zone 2 (2nd column), and Zone 3 (3rd column), from 4 days before the onset of each HW to 4 days after (Lag −4, Lag −2, Lag 0, Lag 2, Lag 4). Deseasonalized MSLP anomalies are shown in contours, and wind directions are indicated by arrows.

In Figure 11, we present the time-shifted composite Tn-HW anomalies for Zones 1, 2, and 3. The results reveal a positive dust anomaly over Senegal four days prior to the onset of HW in Zone 1. This anomaly intensifies at Lag −2, with a more pronounced signal in northwestern Senegal and along the Senegal–Mauritania coast. The signal persists until Lag 0 and gradually weakens between Lags 2 and 4, migrating further north. Fluctuations in MSLP over the ocean, combined with northerly to northeasterly winds over the continent,

are responsible for transporting large quantities of dust from the source regions to Senegal. These findings underscore the role of dust in both triggering and maintaining HW episodes.

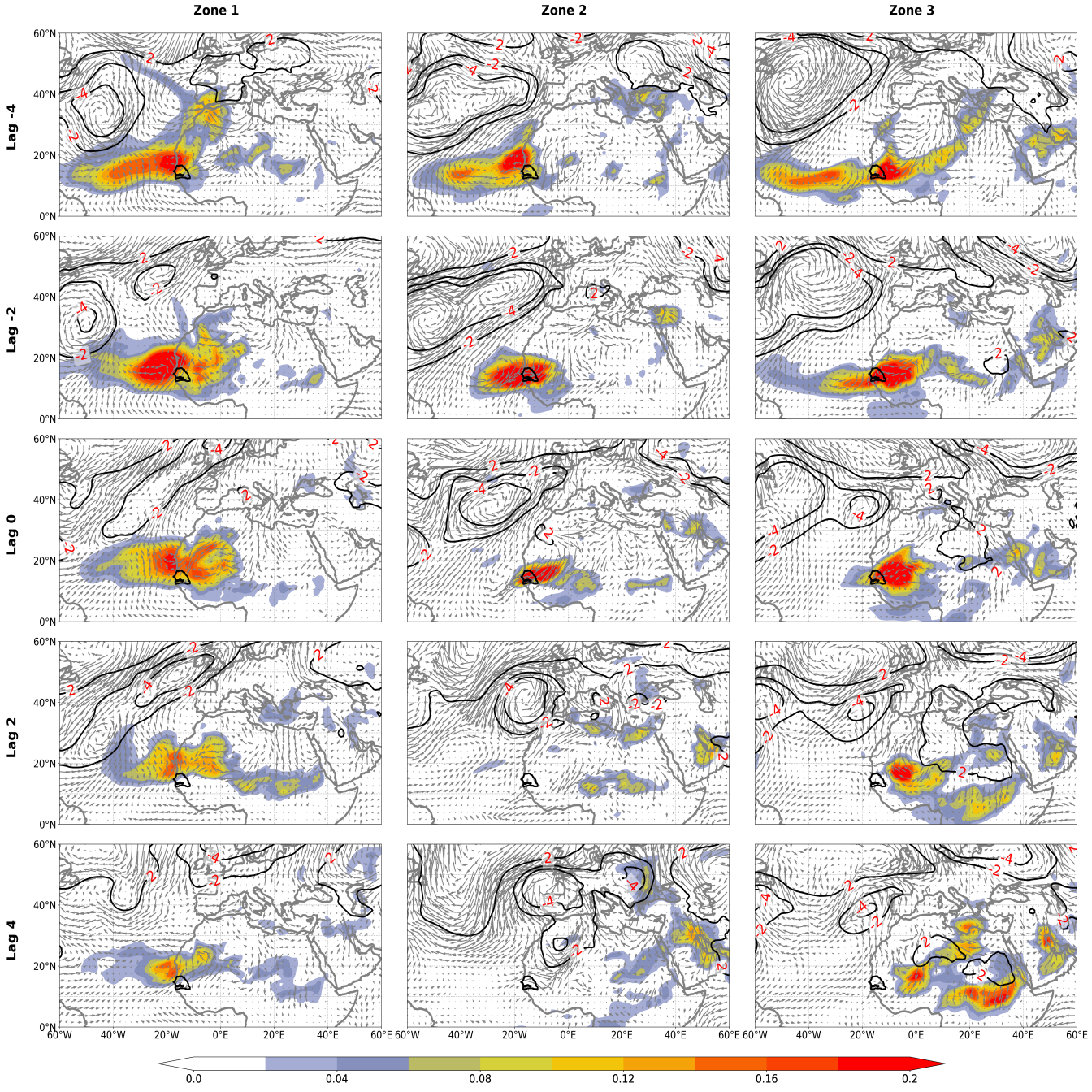

Figure 11. Composite of deseasonalized anomalies of Dust AOD during Tn-HW for Zone 1 (1st column), Zone 2 (2nd column), and Zone 3 (3rd column), from 4 days before the onset of each HW to 4 days after (Lag −4, Lag −2, Lag 0, Lag 2, Lag 4). Deseasonalized MSLP anomalies are shown in contours, and wind directions are indicated by arrows.

Regarding the prolongation of HWs, the results show that dust anomalies begin to diminish after Lag 0 and continue to decrease between Lags 2 and 4. This gradual dissipation of dust seems to correspond to the attenuation of the HW. This suggests that, while dust plays a critical role in initiating and sustaining HW events, its influence wanes over time. Four days before the onset of the HW, a strong dust signal is observed over Senegal, the surrounding ocean, and all bordering countries. By Lag −2, the spatial extent of the signal is reduced, but it strengthens over Senegal. At Lag 0, the positive anomaly

remains over Senegal but dissipates after two days. This positive Dust AOD anomaly over Senegal results from surface pressure fluctuations in the North Atlantic, which increase southerly winds that carry dust further north. Concurrently, north to northeasterly winds from the source regions in Mali and Mauritania transport large quantities of dust.

For the Dust AOD composites associated with Tn-HW in Zone 3, the positive dust anomaly observed at Lag 0 was already present four days earlier (Lag −4), although with a less pronounced spatial extent. However, dust does not appear to contribute to the prolongation of HW duration, as no positive anomaly is detected over Senegal at Lag 2. Similar patterns were observed in the time-lagged composites for Ta-HW (see Figure S9). Additionally, the patterns obtained from Dust AOD were consistent with those for PM2.5 and PM10 (see Figures S10 and S11).

In summary, the results indicate that, while dust plays a significant role in triggering Tn-HW events in Zones 1, 2, and 3, its influence on prolonging these events is limited and varies between zones. MSLP fluctuations and wind patterns are key factors in dust transport and its impact on Tn-HW. Our findings align with those of Niane et al. [51], who analyzed a historical HW event in the Sahel (17–22 April 2010). Their study highlighted an increase in PM10 concentrations, reaching over 500 $\mu g/m^3$, likely due to dust originating from the eastern Libyan Desert. Transported by the Harmattan winds, this dust remained elevated 2 to 3 days prior to the event, maintained high concentrations during the event, and decreased afterward. The interaction between this dust and atmospheric circulation—particularly the winds and an anticyclonic circulation—amplified the warming effect.

3.3.2. Regression Analysis Associated with Temperature Variability

We conducted regressions of the deseasonalized anomalies of wind fields, MSLP, and Dust AOD on the standardized minimum (Tn) and maximum (Tx) temperature indices for the three zones of Senegal during the spring period from 2003 to 2022. The objective was to determine whether the composite anomalies associated with HW align with broader variability patterns influencing overall temperature fluctuations in Senegal.

The regression results for the Tn index reveal complex atmospheric pressure anomalies and dust transport patterns (Figure 12). In Zone 1, the pressure anomalies exhibit a distinct dipole, with negative pressures centered around 35° N, 35° W in the Atlantic Ocean and positive pressures over North Africa (around 35° N, 10° W). This configuration is linked to an atmospheric circulation that favors the transport of drier air masses towards Senegal, thereby elevating minimum temperatures. This mechanism is compounded by increased dust concentrations in Senegal and surrounding regions—particularly in the Sahara and the Sahel—further exacerbating the increase in temperatures. In Zone 2, similar pressure anomalies (although slightly displaced) were also found to influence the minimum temperatures. Increased dust concentrations were observed in areas south of the Sahara, in Senegal, and in the Atlantic Ocean. In Zone 3, the pressure anomalies are more diffuse and closer to the continent, with the positive anomalies previously seen around 10° N, 30° W in Zones 1 and 2 no longer present. Despite this, limited dust dispersion is observed over Senegal and the central West African region. This suggests that Tn in Zone 3 is modulated by more varied atmospheric influences, although dust remains a significant contributing factor. The relationships between deseasonalized PM2.5 and PM10 anomalies and the standardized Tn indices in the three zones were found to follow similar patterns to those observed for Dust AOD (see Figure S12).

For maximum temperatures (Tx), the regressions revealed a significant influence of pressure anomalies and dust transport across the different zones (Figure 13). In Zone 1, we observe the same dipole pattern found in the Tn regression, accompanied by dust concentrations spanning a broad Sahelian band and the Atlantic Ocean, particularly along the Senegalese coast. This indicates the transport of Saharan dust towards Senegal, driven by high-pressure systems centered around 10° N, 30° W, resulting in an increase in maximum temperatures.

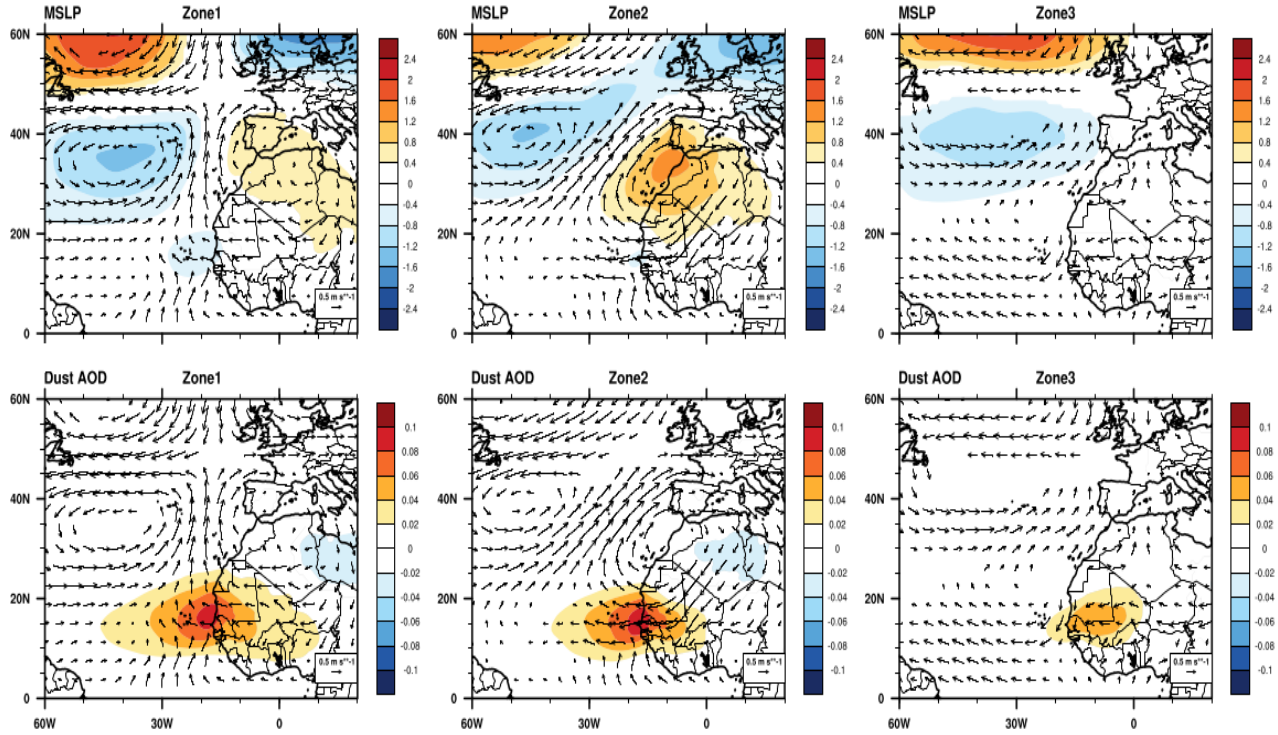

Figure 12. Regression of deseasonalized anomalies of MSLP (1st row) and Dust AOD (2nd row) on Tn standardized indices in Zones 1, 2, and 3 during spring (MAM) 2003–2022. Arrows indicate the direction of the regressed wind fields. Statistically significant results at the 95% confidence level are highlighted.

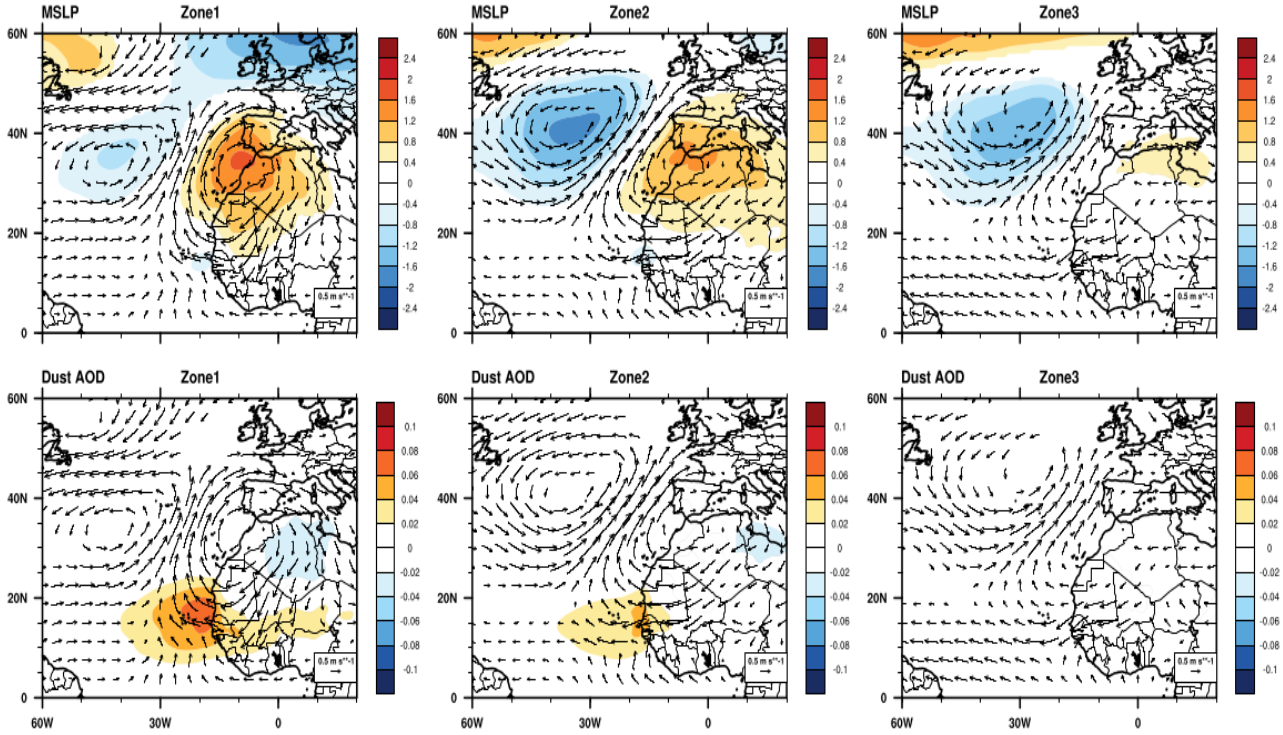

Figure 13. Regression of deseasonalized anomalies of MSLP (1st row) and Dust AOD (2nd row) on Tx standardized indices in Zones 1, 2, and 3 during spring (MAM) 2003–2022. Arrows indicate the direction of the regressed wind fields. Statistically significant results at the 95% confidence level are highlighted.

In Zone 2, the positive pressure anomalies shift slightly northward (approximately 40° N, 30° W), and the positive anomalies move eastward over North Africa. While dust transport becomes more localized, concentrations continue to influence maximum temperatures, especially in Senegal. In Zone 3, the positive pressure anomalies shift significantly (35° N, 10° E), although they are less pronounced. The absence of Saharan dust in Senegal suggests that maximum temperatures in this zone are influenced by more localized mechanisms, such as atmospheric instability and local heat flows. Regressions of deseasonalized anomalies of PM2.5 and PM10 on the standardized Tx indices across the three zones exhibited patterns similar to those for Dust AOD (see Figure S13).

The results of Sambou et al. [52] revealed a similar pattern. Intra-seasonal temperature variations in Senegal, whether increasing or decreasing, are closely linked to recurrent atmospheric pressure dynamics centered around the Strait of Gibraltar. This phenomenon is particularly pronounced in Zones 1 and 2. In contrast, temperature fluctuations in Zone 3 tend to be relatively limited.

Our analyses demonstrated that the composite anomalies associated with HWs—whether concerning Tn or Tx—align with a broader variability mode influencing temperature patterns in Senegal. Atmospheric pressure anomalies and dust transport play critical roles in modulating temperatures, with significant impacts on the variations in Tn and Tx across the different zones. The obtained results, which emphasize the influence of dust anomalies, support recent findings indicating that HWs in Zones 1 and 2 are more closely associated with dust than those in Zone 3. Additionally, Tn-HW showed a stronger connection to dust when compared to Tx-HW (see Figure 9).

3.4. Relationship Between Aerosol Diurnal Cycle and Heat Waves

Figure 14 illustrates the concentrations of PM2.5 and wind anomalies at 925 hPa at various times of the day (00:00, 03:00, 06:00, 09:00, 12:00, 15:00, 18:00, and 21:00 UTC) in Senegal during the spring period from 2003 to 2022. The reference stations, marked by stars on the maps, allow for precise tracking of concentration variations at these locations. Hovmöller diagrams depicting the magnitude of wind anomalies for the regions 15° N–17.5° N and 12° N–14.5° N, respectively, for the same period and season are also presented in Figure 14b and Figure 14c, respectively. In addition to the spatial distribution of the diurnal cycle of PM2.5 concentrations and wind anomalies, we also provide a figure illustrating the baseline wind patterns (without anomalies) for the same period (see Figure S14). This figure enables a clearer understanding of the prevailing wind directions during spring (March–May) from 2003 to 2022, and highlights the importance of comparison with wind anomalies.

The diurnal cycle of PM2.5 concentrations varies significantly across stations, being influenced by local geography, proximity to desert dust sources, atmospheric conditions, and wind patterns. The results indicate that maximum PM2.5 concentrations during the spring occur between night and morning (00:00 to 09:00 UTC). This phenomenon is primarily driven by two mechanisms. First, the atmospheric stability during night, characterized by thermal inversions near the surface, limits particle dispersion and promotes their accumulation. This effect is particularly pronounced in the northern and northeastern regions of Senegal, near desert dust sources; especially in Podor, Linguère, Matam, and parts of Saint-Louis. Second, the generally weak night-time winds (see Figure 14c) transport Saharan dust to these areas, and thermal inversion prevents vertical dispersion, thus maintaining high PM2.5 concentrations near the surface. Stations in Zone 1 experience an influx of sea salts, particularly between 00:00 and 03:00 UTC. These marine aerosols, transported by ocean winds, interact with PM2.5, influencing particle levels in these stations. Winds along the 15° N–17.5° N axis (Figure 14b) are weaker, compared to those along the 12° N–14.5° N axis (Figure 14c), meaning that the transport of marine aerosols, especially towards Saint-Louis, is less effective due to weaker winds. In contrast, stations farther south, such as Dakar-Yoff and Cap Skirring, benefit from stronger transport.

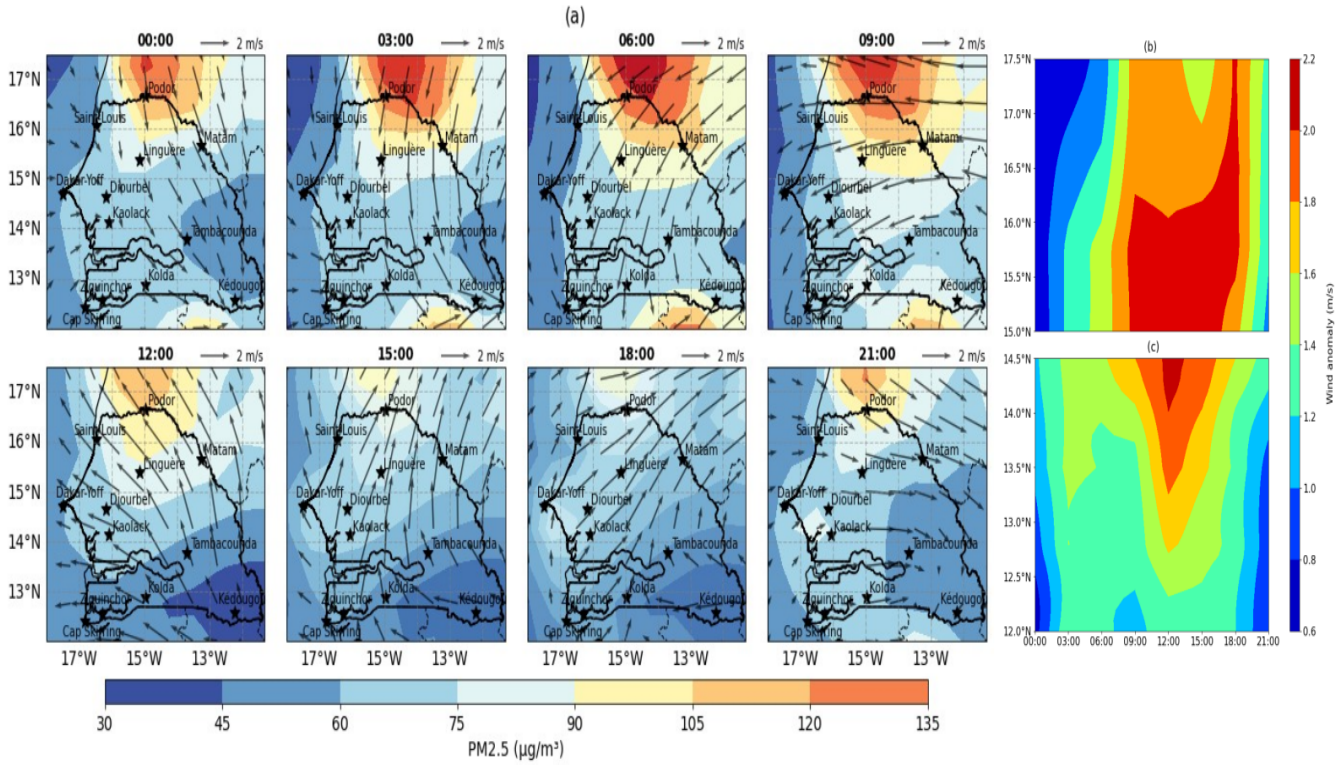

Figure 14. (**a**) Spatial distribution of the diurnal cycle of PM2.5 concentrations (µg/m^3) in Senegal during spring (March–May) from 2003 to 2022, with reference station locations marked by stars on the map and wind anomalies represented by arrows. (**b**,**c**) Hovmöller diagrams of wind anomaly magnitude at 925 hPa for the regions 15° N–17.5° N and 12° N–14.5° N, respectively, during the same season and period.

Between 12:00 and 18:00 UTC, a notable decrease in PM2.5 concentrations is observed at northern stations, partly due to increased daytime convection, which facilitates particle dispersion. Stronger daytime winds, originating from the south and being more humid, also transport anthropogenic particles. Human activities, such as traffic and industrial emissions, contribute significantly to the increase in PM2.5 concentrations during the day. Additionally, higher daytime temperatures induce greater atmospheric turbulence (Figure 14b,c), facilitating particle dispersion and reducing concentrations near the ground. The diurnal cycle of desert dust in the Sahel has been insufficiently documented due to the lack of continuous observations throughout the day. To address this gap, Mbourou et al. [85] calculated the annual number of days when visibility drops below 5 and 10 km at each synoptic hour across nine stations spanning from the equator to North Africa. Their findings suggest that diurnal changes in surface thermal inversion and surface winds intensify the diurnal cycle of dust frequency in central Sahel stations. This aligns with our results, highlighting how night-time stability and weak winds contribute to the accumulation of PM2.5, while daytime convection and increased turbulence enhance dispersion.

We also produced similar figures for PM10 and Dust AOD (see Figures S15 and S16, respectively), which display patterns comparable to those observed for PM2.5. These supplementary figures further support our findings regarding the diurnal cycle of particulate matter and its relationship with desert dust in Senegal. The consistency across PM2.5, PM10, and Dust AOD suggests that similar atmospheric dynamics govern their behavior, particularly in relation to night-time stability, thermal inversions, and daytime convection.

This dynamic of the diurnal cycle of particulate matter and Dust AOD provides insight into the varying associations between aerosol levels and HWs. Tn-HW appears to be more strongly correlated with high aerosol levels than Tx-HW, which may be attributed to the nocturnal accumulation of aerosols under conditions of atmospheric stability, which

enhances Tn-HW through limiting radiative cooling. Conversely, during the day, aerosol dispersion through convection reduces their impact on daytime HWs.

4. Discussion

4.1. Impact of Aerosols on Heat Waves in Senegal

In this study, we examine the effects of modulation of various types of aerosols (PM2.5, PM10, AOD, and Dust AOD) on HWs in Senegal. Our composite analyses for HWs did not reveal any significant patterns that differentiate the types of aerosols (Figure 8). Consequently, it appears that aerosols, regardless of their type, do not distinctly influence HWs in Senegal. These results seem to corroborate the conclusions of Sousa et al. [49], who demonstrated that substantial volumes of dust and other aerosols are transported by Saharan intrusions to mid-latitudes, as observed during the 2018 HW over the Iberian Peninsula. Their work highlighted the potential warming effect due to the concentration of aerosols at the surface during HWs.

We found that the influence of aerosols on HWs varies by region. Zone 1, which is influenced by both sea salts and Saharan dust, experiences a greater impact of HWs. The higher concentration of aerosols in the atmosphere increases radiative absorption, thereby raising temperatures. Prevailing spring winds facilitate the transport of Saharan dust to these coastal regions, amplifying the concentrations of aerosols and intensifying the effects of HWs. In contrast, Zones 2 and 3 presented a lesser influence of aerosols on HWs, suggesting that other factors may play more prominent roles in these areas. These findings highlight the importance of considering local meteorological conditions and geographical features to fully understand their impacts on HWs.

Additionally, we analyzed the differences between Tx-HW, Tn-HW, and Ta-HW in relation to aerosols. Our results indicate that Tn-HWs and Ta-HWs are associated with high aerosol concentrations in Senegal, whereas Tx-HWs are not consistently linked with high aerosol levels (Figures 8 and 9). These findings are consistent with those of [86], who differentiated daytime HWs (associated with lower aerosol loads) from night-time HWs (characterized by higher aerosol loads). Furthermore, [87] showed that desert aerosols are linked to a reduction in solar radiation reaching the surface, leading to cooler daytime temperatures. On the other hand, dust retains thermal radiation in the lower troposphere, which contributes to an increase in surface air temperature at night [88]. Niane et al. [51] assessed the impact of mineral aerosols, which are commonly present in Sahelian HWs from March to June. Their results demonstrated that pure dust-type HWs (Type 1: $AOD_{550} \geq 1$ and $AE_{440–870} < 0.5$) are more intense, highlighting their potential local warming effect. Mixed-dust HWs (Type 2: $AOD_{550} < 1$ and $AE_{440–870} < 0.5$, and Type 3: $AOD_{550} < 1$ and $AE_{440–870} \geq 0.5$), although present, are less intense. Recent research conducted by [48] in southern Europe revealed that mineral dust can locally alter the solar radiation reaching the surface. The authors observed that an increase in aerosol concentration led to a significant radiative cooling effect at short wavelengths at the Évora station in southern Portugal. However, this effect was offset by longwave radiative warming at the surface. Despite this, estimation of the radiative forcing associated with dust particles remains complex [89], mainly due to the lack of simultaneous measurements at short and long wavelengths, especially during dust events. The work of [49] highlighted the correlation between HW episodes in Spain in 2018 and 2019 and the arrival of warm air masses containing above-average concentrations of Saharan dust. These observations suggest that these events could influence surface temperatures. However, other studies have shown that desert dust tends to exert a net negative radiative impact, contributing to a cooling trend in surface temperatures in West Africa [90]. In the Sahel, ref. [50] demonstrated that the accumulation of mineral dust in the atmosphere leads to decreases in the frequencies of hot days, very hot days, and hot nights.

4.2. Diurnal Variation

We demonstrated that, in spring, Tn-HWs appear to be more strongly correlated with high dust levels than Tx-HWs, due to the nocturnal accumulation of aerosols (between 00:00 and 09:00 UTC) under stable atmospheric conditions (Figure 14). These findings are consistent with those of Cowie et al. [91], who observed a peak in dust events at 9 a.m. in the central Sahel, indicating a strong influence of the nocturnal low-level jet (NLLJ). The NLLJ, which forms south of the Sahara and north of the Sahel during the dry season, plays a crucial role in transporting dust toward the Sahel.

These results differ from those of Mbourou et al. [85], who studied the diurnal dust cycle throughout the entire year—not just in spring—and found that dust concentrations peaked around noon. Ozer [92] also demonstrated that dust events are most intense during the day, particularly between 9 a.m. and 3 p.m., and are at their lowest at night. Additionally, Kaly et al. [64] confirmed this diurnal cycle, with peak wind speeds generally observed between 10 a.m. and 12 p.m. UTC, corresponding with similar peaks in PM10 concentrations.

Further studies are necessary to explore the meteorological conditions associated with dusty HWs in Senegal, and to better understand how physical processes shape both night-time and daytime temperatures during these events. Analyzing dusty HWs in a manner coupled with high-resolution observations and simulations, and investigating the interactions between dust levels and HW characteristics, will be key to advancing this understanding.

To fully assess the consequences of dust-related HWs in Senegal, it is crucial to consider the population's exposure to fine particulate matter (PM), such as PM10 and PM2.5. High concentrations of desert dust not only influence temperatures during HWs, but also significantly impact air quality, particularly in urban areas. Previous studies have shown that unhealthy and even hazardous PM levels are common during the dry season (winter/spring), while dust concentrations are substantially lower during the summer months [37,47]. Additionally, unpublished medical studies from Senegal have emphasized the increased prevalence of non-vector diseases (e.g., acute respiratory infections, asthma, bronchitis, and cardiovascular diseases) and vector-borne diseases (e.g., tuberculosis) during the dry season. The following section examines the effects of prolonged exposure to fine particles on public health in Senegal, emphasizing the heightened risks during extreme heat events, in line with our study's findings on spring HWs.

4.3. Spatial Distribution of Spring PM Exposure in Senegal

Figure 15 shows the spatial distribution of the percentage of days with unhealthy PM2.5 and PM10 concentrations (i.e., above the threshold values) during the spring season (MAM) from 2003 to 2022, based on Senegalese standards (NS 05-062) from 2019.

Unhealthy PM2.5 concentrations (Figure 15a) are predominantly concentrated in the northern regions of Senegal, particularly in Saint-Louis, Podor, Linguère, and Matam, where the percentage of unhealthy days can exceed 60%. In contrast, stations located further south, such as Tambacounda, Kolda, and Kédougou, exhibit much lower levels, with unhealthy day percentages below 10%. This disparity is largely due to the distance of these areas from the primary sources of Saharan dust, as well as local factors such as vegetation cover.

A similar spatial pattern was observed for PM10 concentrations ($\geq$150 $\mu g/m^3$), with higher levels in the northern regions (Figure 15b). Stations in the south and central regions experience lower pollution levels, reflecting the predominant contribution of desert dust in the northern parts of Senegal. The spring season coincides with an intensification of winds carrying desert dust, leading to elevated PM concentrations at northern stations, especially those near dust source areas in Mauritania.

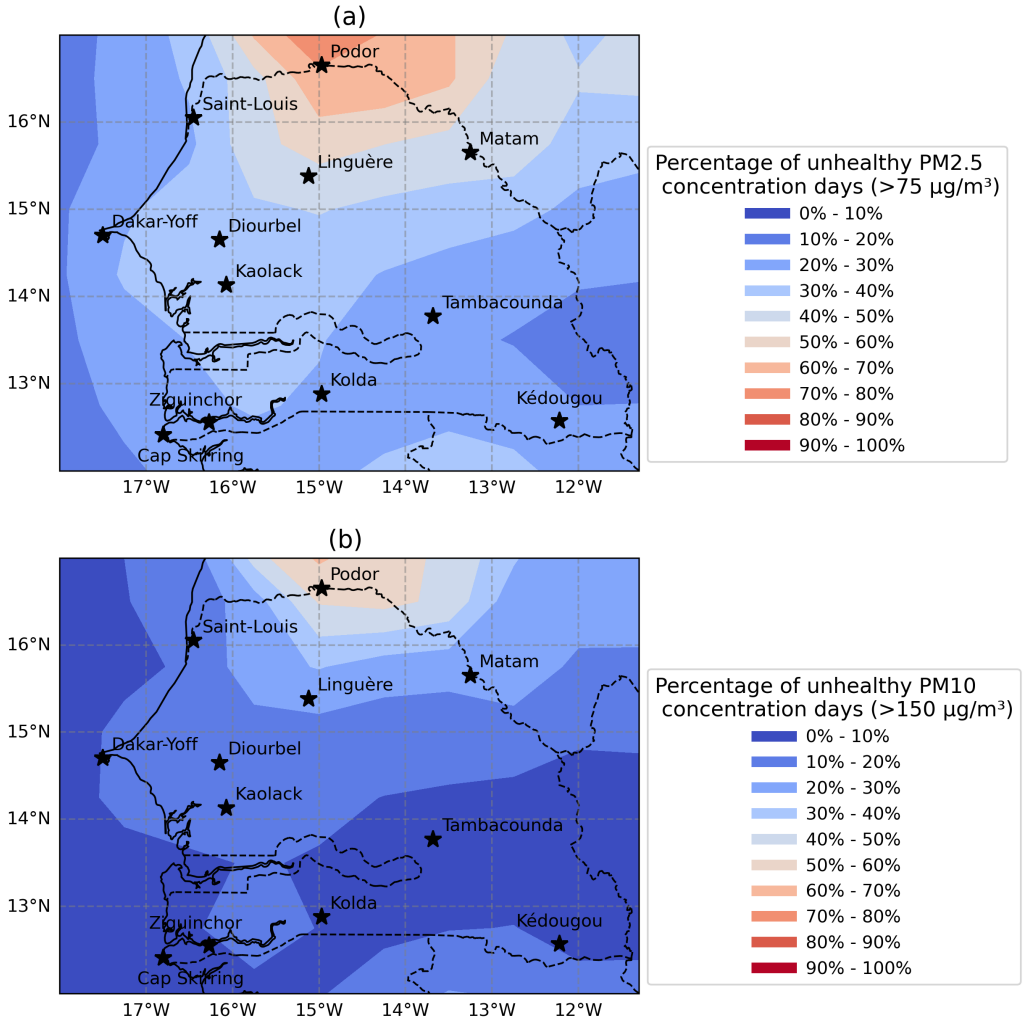

Figure 15. Spatial distribution of the percentage of days with concentrations of unhealthy fine particles in spring (MAM) from 2003 to 2022 in Senegal, according to the NS 05-062 standards: (**a**) PM2.5 (>75 µg/m^3) and (**b**) PM10 (>150 µg/m^3).

These results indicate that the populations of Podor, Linguère, and Matam, who suffer from prolonged exposure to unhealthy particle levels, are particularly vulnerable to respiratory problems and other public health impacts. The young and the elderly are among the most vulnerable groups, due to the heightened sensitivity of their respiratory systems to air pollution. Children, whose lungs and immune systems are still developing, are more likely to suffer from respiratory illnesses, while the elderly, who often have pre-existing health problems, including respiratory and cardiovascular conditions, suffer from amplified effects of particulate exposure. Toure et al. [47] reached similar conclusions in their study of the DJF season (December, January, February), in which they analyzed the percentage of days when simulated PM2.5 and PM10 concentrations exceeded harmful thresholds (>35 µg/m^3 for PM2.5 and 150 µg/m^3 for PM10) across the 14 administrative districts of Senegal for the 2015–2016 period. They found that over 90% of the simulated days in northern districts, such as Saint-Louis and Louga, had PM2.5 levels exceeding moderate thresholds. In the urban districts of Dakar and Diourbel, more than 80% of days had moderate PM2.5 levels. Regarding PM10, concentrations exceeding 150 µg/m^3 were observed on over 90% of days in the northern districts, while southern districts saw moderate PM10 concentrations on 40–60% of days. The spatial patterns of PM10 exposure closely mirror those of PM2.5 across Senegal, with Saint-Louis experiencing the highest exposure. Toure et al. [47] also found that the prevalence of asthma, bronchitis, and acute

respiratory infections was highest among children under 5 years old, particularly in Dakar, while adult women and young people aged 15–25 were also significantly affected. Urban areas showed a stronger association between air pollution and these diseases, while rural areas were less impacted. In a related study, Jenkins et al. [93] simulated a dust episode using the WRF model in 2016, which had a particularly severe impact on the northern and central districts of Senegal. During this event, the district of Saint-Louis—which is home to over one million inhabitants—was exposed to hazardous levels of PM10 for 9 out of 10 observation days. This highlights the severity of air pollution exposure in northern Senegal and underscores the ongoing vulnerability of populations to health issues related to fine particulate matter.

In addition, other environmental factors, such as temperature and humidity, can exacerbate health problems in areas already exposed to high concentrations of fine particles, for example, contributing to increased cases of meningitis [37]. Furthermore, To et al. [94] have shown that these same atmospheric conditions can exacerbate asthma outside the dust season.

The high PM levels observed in Senegal—particularly in the northern region—underline the importance of extending the particulate matter observation network and incorporating other types of pollutants in order to assess their impact on health more accurately.

5. Conclusions and Perspectives

The purpose of this study was to characterize HWs in Senegal using daily maximum, minimum, and apparent temperature data from 12 synoptic stations in the GSOD database over the period from 2003 to 2022. HW detection was conducted based on exceeding the 95th moving percentile of daily air temperatures during the spring season (from March to May), calculated over a 29-day window in order to attenuate the effects of seasonality, in line with the methodology used by Sambou et al. (2019) [52].

A hierarchical cluster analysis identified three homogeneous zones (Zones 1, 2, and 3), stretching from the Atlantic coast inland, each made up of four stations, which were defined according to whether hot days occurred simultaneously between stations.

This study also aimed to understand the mechanisms by which desert dust influences the dynamics of HWs, utilizing reanalysis data from the CAMS service for the study period. Particular attention was paid to the hypothesis that dust loading could have distinct effects on diurnal and nocturnal HW characteristics.

Our results demonstrate that HWs are more frequent in the coastal zone (Zone 1: Saint-Louis, Dakar-Yoff, Cap Skirring, and Ziguinchor) than in the intermediate zone (Zone 2: Podor, Linguère, Diourbel, and Kaolack) and the continental zone (Zone 3: Matam, Tambacounda, Kédougou, and Kolda). HWs associated with minimum temperatures (Tn-HWs) and apparent temperatures (Ta-HWs) are more strongly correlated with high dust concentrations than those associated with maximum temperatures (Tx-HWs). Specifically, Tn-HWs are strongly influenced by the accumulation of aerosols during night-time under stable atmospheric conditions.

The mechanisms linking HWs to dust show that dust is present in Senegal and its neighboring regions four days before the onset of an HW. These dust anomalies persist until the beginning of the HW and disappear two days after. The presence of dust in Senegal is associated with a positive pressure anomaly in Europe at Lag −4, which gradually shifts towards North Africa by Lag 0, generating north winds that transport dust towards Senegal. The highest concentrations of PM and AOD linked to dust in Senegal are observed in spring, between midnight and the morning (00:00 to 09:00 UTC). This diurnal pattern underscores the differences in how aerosol levels relate to HWs, depending on whether the HW is associated with Tx or Tn.

Finally, this study highlights the severity of exposure to fine particulate pollution in northern Senegal, emphasizing the persistent vulnerability of populations to health issues related to these particles. These findings underscore the importance of developing adaptation and prevention strategies tailored to the most vulnerable regions of Senegal. The

combination of HWs and desert dust episodes represents a major health risk, particularly for fragile and vulnerable populations.

This study contributes to a better understanding of climate–aerosol interactions, which are essential for addressing current and future climate challenges. Further research is needed to explore the weather conditions associated with dusty HWs in Senegal in greater depth, as well as to better understand how physical processes influence night-time and daytime temperatures during these phenomena.

Supplementary Materials: The following supporting information can be downloaded at https://www.mdpi.com/article/10.3390/atmos15121413/s1: Figure S1: Seasonal cycles of Dust AOD (grey bars) and temperatures (Tx in red, Tn in blue, Ta in green) in 12 stations across Senegal. Stations are ordered (from left to right, from top to bottom) by decreasing dust concentrations; Figure S2: Seasonal cycles of PM10 (grey bars) and temperatures (Tx in red, Tn in blue, Ta in green) in 12 stations across Senegal. Stations are ordered (from left to right, from top to bottom) by decreasing PM10 concentrations ($\mu g/m^3$); Figure S3: Evolution of Tx-HW (1st row), Tn-HW (2nd row) and Ta-HW (3rd row) for Zone 1 (1st column), Zone 2 (2nd column) and Zone 3 (3rd column) from 2003 to 2022; Figure S4: Composite of deseasonalized anomalies of PM2.5 ($\mu g/m^3$) for Tx-HW (1st row), Tn-HW (2nd row) and Ta-HW (3rd row) from Zone 1 (1st column), Zone 2 (2nd column) and Zone 3 (3rd column) in Senegal; Figure S5: Composite of deseasonalized anomalies of PM10 ($\mu g/m^3$) for Tx-HW (1st row), Tn-HW (2nd row) and Ta-HW (3rd row) from Zone 1 (1st column), Zone 2 (2nd column) and Zone 3 (3rd column) in Senegal; Figure S6: Composite of deseasonalized anomalies of AOD for Tx-HW (1st row), Tn-HW (2nd row) and Ta-HW (3rd row) from Zone 1 (1st column), Zone 2 (2nd column) and Zone 3 (3rd column) in Senegal; Figure S7: Composite of deseasonalized anomalies of PM2.5 ($\mu g/m^3$) during Tx-HW for Zone 1 (1st column), Zone 2 (2nd column), and Zone 3 (3rd column), from 4 days before the onset of each HW to 4 days after (Lag −4, Lag −2, Lag 0, Lag 2, Lag 4); Figure S8: Composite of deseasonalized anomalies of PM10 ($\mu g/m^3$) during Tx-HW for Zone 1 (1st column), Zone 2 (2nd column), and Zone 3 (3rd column), from 4 days before the onset of each HW to 4 days after (Lag −4, Lag −2, Lag 0, Lag 2, Lag 4); Figure S9: Composite of deseasonalized anomalies of Dust AOD during Ta-HW for Zone 1 (1st column), Zone 2 (2nd column), and Zone 3 (3rd column), from 4 days before the onset of each HW to 4 days after (Lag −4, Lag −2, Lag 0, Lag 2, Lag 4); Figure S10: Composite of deseasonalized anomalies of PM2.5 ($\mu g/m^3$) during Tn-HW for Zone 1 (1st column), Zone 2 (2nd column), and Zone 3 (3rd column), from 4 days before the onset of each HW to 4 days after (Lag −4, Lag −2, Lag 0, Lag 2, Lag 4); Figure S11: Composite of deseasonalized anomalies of PM10 ($\mu g/m^3$) during Tn-HW for Zone 1 (1st column), Zone 2 (2nd column), and Zone 3 (3rd column), from 4 days before the onset of each HW to 4 days after (Lag −4, Lag −2, Lag 0, Lag 2, Lag 4); Figure S12: Regression of deseasonalized anomalies of PM2.5 & PM10 ($\mu g/m^3$) on Tn standardized indices in Zone 1 (1st column), Zone 2 (2nd column), and Zone 3 (3rd column) during spring (MAM) 2003–2022. Arrows indicate the direction of the regressed wind fields. Statistically significant results at 95% confidence level are highlighted; Figure S13: Regression of deseasonalized anomalies of PM2.5 & PM10 ($\mu g/m^3$) on Tx standardized indices in Zone 1 (1st column), Zone 2 (2nd column), and Zone 3 (3rd column) during spring (MAM) 2003–2022. Arrows indicate the direction of the regressed wind fields. Statistically significant results at 95% confidence level are highlighted; Figure S14: Spatial distribution of diurnal cycle of PM2.5 ($\mu g/m^3$) in Senegal during spring (March–May) from 2003 to 2022, with reference station locations marked by stars on the map and wind direction represented by arrows; Figure S15: Spatial distribution of diurnal cycle of PM10 ($\mu g/m^3$) in Senegal during spring (March–May) from 2003 to 2022, with reference station locations marked by stars on the map and wind anomalies represented by arrows; Figure S16: Spatial distribution of diurnal cycle of Dust AOD in Senegal during spring (March–May) from 2003 to 2022, with reference station locations marked by stars on the map and wind anomalies represented by arrows; Table S1: Location of PurpleAir sensors for the Jeune Équipe Associée à l'IRD Climat et Santé au Sénégal (JEAI-CLISAS) project.

Author Contributions: Conceptualization, S.D. and A.D.; methodology, S.D., A.D. and M.-J.G.S.; software, S.D.; data curation, S.D.; visualization, S.D.; supervision, A.D., S.J. and J.M.; writing—original draft, S.D.; writing—review and editing, A.D., P.F., D.G., S.J., J.M. and M.-J.G.S.; funding acquisition, A.D. All authors have read and agreed to the published version of the manuscript.

Funding: This study is part of the ANR project ACASIS (2014–2018, grant: ANR-13-SENV-0007) and the JEAI IRD program through JEAI-CLISAS (Young Team Associated with IRD Climate and Health in Senegal). This work is also supported by LMI-ECLAIRS-2, which focuses on integrated studies of climate and ocean in West Africa and responses to climate change in Senegal. The funders played no role in determining the study design, selecting the data collection or analysis methods employed, the decision to publish, or the preparation of the paper.

Institutional Review Board Statement: Not applicable.

Informed Consent Statement: Not applicable.

Data Availability Statement: The in situ temperature data used in this work were obtained from the Global Surface Summary of the Day (GSOD) database produced by the National Climatic Data Center (NCDC). Data were downloaded from https://catalog.data.gov/dataset/global-surface-summary-of-the-day-gsod1, accessed on 4 January 2024. In situ aerosol data from the INDAAF network are available at https://indaaf.obs-mip.fr/catalogue/, accessed on 13 February 2024. In situ aerosol data from the AERONET network are available at https://aeronet.gsfc.nasa.gov/new_web/draw_map_display_aod_v3.html, accessed on 20 February 2024. Reanalysis data from CAMS are available at https://ads.atmosphere.copernicus.eu/cdsapp#!/dataset/cams-global-reanalysis-eac4?tab=form, accessed on 14 March 2024. The sharing of data from the PurpleAir network in Saint-Louis is not applicable to this article.

Acknowledgments: The authors acknowledge the French and African PIs and operators for maintaining the INDAAF stations. We also thank the National Climatic Data Center (NCDC) for maintaining the GSOD stations, LISA for their efforts in establishing and maintaining the AERONET sites in Senegal, and COPERNICUS for the CAMS reanalyses. We would like to express our sincere gratitude to Serigne Bassirou DIOP for producing the map in Figure 2 and Ibrahima Diouf for his valuable assistance in proofreading the manuscript.

Conflicts of Interest: The authors declare no conflicts of interest.

References

1. Intergovernmental Panel on Climate Change (IPCC). *Global Warming of 1.5 °C. An IPCC Special Report on the Impacts of Global Warming of 1.5 °C Above Pre-Industrial Levels and Related Global Greenhouse Gas Emission Pathways, in the Context of Strengthening the Global Response to the Threat of Climate Change, Sustainable Development, and Efforts to Eradicate Poverty*; Masson-Delmotte, V., Zhai, P., Pörtner, H.-O., Roberts, D., Skea, J., Shukla, P.R., Pirani, A., Moufouma-Okia, W., Péan, C., Pidcock, R., et al., Eds.; World Meteorological Organization: Geneva, Switzerland, 2018; p. 32.
2. Eyring, V.; Gillett, N.P.; Rao, K.M.A.; Barimalala, R.; Parrillo, M.B.; Bellouin, N.; Cassou, C.; Durack, P.J.; Kosaka, Y.; McGregor, S.; et al. Human Influence on the Climate System. In *Climate Change 2021: The Physical Science Basis. Contribution of Working Group I to the Sixth Assessment Report of the Intergovernmental Panel on Climate Change*; Masson-Delmotte, V., Zhai, P., Pirani, A., Connors, S.L., Péan, C., Berger, S., Caud, N., Chen, Y., Goldfarb, L., Gomis, M.I., et al., Eds.; Cambridge University Press: Cambridge, UK; New York, NY, USA, 2021; pp. 423–552.
3. Russo, S.; Dosio, A.; Graversen, R.G.; Sillmann, J.; Carrao, H.; Dunbar, M.B.; Singleton, A.; Montagna, P.; Barbola, P.; Vogt, J.V. Magnitude of extreme heat waves in present climate and their projection in a warming world. *J. Geophys. Res. Atmos.* **2014**, *119*, 12–500. [CrossRef]
4. Oueslati, B.; Pohl, B.; Moron, V.; Rome, S.; Janicot, S. Characterization of heat waves in the Sahel and associated physical mechanisms. *J. Clim.* **2017**, *30*, 3095–3115. [CrossRef]
5. Ngoungue Langue, C.G.; Lavaysse, C.; Vrac, M.; Flamant, C. Heat Wave Monitoring over West African Cities: Uncertainties, Characterization and Recent Trends. *Nat. Hazards Earth Syst. Sci.* **2023**, *23*, 1313–1333. [CrossRef]
6. Fischer, E.M.; Knutti, R. Anthropogenic contribution to global occurrence of heavy-precipitation and high-temperature extremes. *Nat. Clim. Chang.* **2015**, *5*, 560–564. [CrossRef]
7. Perkins, S.E. A review on the scientific understanding of heatwaves-Their measurement, driving mechanisms, and changes at the global scale. *Atmos. Res.* **2015**, *164–165*, 242–267. [CrossRef]
8. Rome, S.; Pohl, B.; Oueslati, B.; Moron, V.; Raymond, F.; Janicot, S.; Diedhou, A. Durée et fréquence des vagues de chaleur en Afrique tropicale septentrionale selon 5 indices de chaleur. In *Le Changement Climatique, la Variabilité et les Risques Climatiques Climatic Change, Variability and Climatic Risks*; Université Aristote: Thessaloniki, Greece, 2019; pp. 284–289.
9. Dematte, J.E.; O'Mara, K.; Buescher, J.; Whitney, C.G.; Forsythe, S.; McNamee, T.; Adiga, R.B.; Ndukwu, I.M. Near-fatal heat stroke during the 1995 heat wave in Chicago. *Ann. Intern. Med.* **1998**, *129*, 173–181. [CrossRef] [PubMed]
10. Coumou, D.; Rahmstorf, S. A Decade of Weather Extremes. *Nat. Clim. Chang.* **2012**, *2*, 491–496. [CrossRef]

11. Shaposhnikov, D.; Revich, B.; Bellander, T.; Bedada, G.B.; Bottai, M.; Kharkova, T.; Kvasha, E.; Lezina, E.; Lind, T.; Pershagen, G.; et al. Mortality Related to Air Pollution with the Moscow Heat Wave and Wildfire of 2010. *Epidemiology* **2014**, *25*, 359–364. [CrossRef]
12. Barbier, J. Extrêmes Climatiques-Les Vagues de Chaleur au Printemps sahéLien. Doctoral Dissertation, Institut National Polytechnique de Toulouse-INPT, Toulouse, France, 2017.
13. Barry, A. Incidences sanitaires de la vague de chaleur du mois de Mai 2013 dans les départements de Dagana et de Podor: Analyse géographique. Master's Thesis, Sociétés et Développement, UCAD, Dakar, Senegal, 2015.
14. Sy, I.; Cisse, B.; Ndao, B.; Toure, M.; Diouf, A.A.; Sarr, M.A.; Ndione, J.A. Heat waves and health risks in the northern part of Senegal: Analyzing the distribution of temperature-related diseases and associated risk factors. *Environ. Sci. Pollut. Res.* **2022**, *29*, 83365–83377. [CrossRef]
15. Forster, P.; Ramaswamy, V.; Artaxo, P.; Berntsen, T.; Betts, R.; Fahey, D.W.; Haywood, J.; Lean, J.; Lowe, D.C.; Myhre, G.; et al. Changes in atmospheric constituents and in radiative forcing. In *Climate Change 2007: The Physical Science Basis. Contribution of Working Group I to the Fourth Assessment Report of the Intergovernmental Panel on Climate Change*; Solomon, S., Qin, D., Manning, M., Chen, Z., Marquis, M., Averyt, K.B., Tignor, M., Miller, H.L., Eds.; Cambridge University Press: Cambridge, UK; New York, NY, USA, 2007; pp. 129–234.
16. Engelstaedter, S.; Tegen, I.; Washington, R. North African dust emissions and transport. *Earth-Sci. Rev.* **2006**, *79*, 73–100. [CrossRef]
17. Formenti, P.; Schütz, L.; Balkanski, Y.; Desboeufs, K.; Ebert, M.; Kandler, K.; Petzold, A.; Scheuvens, D.; Weinbruch, S.; Zhang, D. Recent progress in understanding physical and chemical properties of African and Asian mineral dust. *Atmos. Chem. Phys.* **2011**, *11*, 8231–8256. [CrossRef]
18. Pierre, C.; Bergametti, G.; Marticorena, B.; Abdourhamane Touré, A.; Rajot, J.L.; Kergoat, L. Modeling wind erosion flux and its seasonality from a cultivated Sahelian surface: A case study in Niger. *Catena* **2014**, *122*, 61–71. [CrossRef]
19. d'Almeida, G.A. A model for Saharan dust transport. *J. Appl. Meteorol. Climatol.* **1986**, *25*, 903–916. [CrossRef]
20. Kaufman, Y.J.; Koren, I.; Remer, L.A.; Tanré, D.; Ginoux, P.; Fan, S. Dust transport and deposition observed from the Terra-Moderate Resolution Imaging Spectroradiometer (MODIS) spacecraft over the Atlantic Ocean. *J. Geophys. Res. Atmos.* **2005**, *110*. [CrossRef]
21. Prospero, J.M.; Bonatti, E.; Schubert, C.; Carlson, T.N. Dust in the Caribbean atmosphere traced to an African dust storm. *Earth Planet. Sci. Lett.* **1970**, *9*, 287–293. [CrossRef]
22. Chiapello, I.; Bergametti, G.; Gomes, L.; Chatenet, B.; Dulac, F.; Pimenta, J.; Suares, E.S. An additional low layer transport of Sahelian and Saharan dust over the northeastern tropical Atlantic. *Geophys. Res. Lett.* **1995**, *22*, 3191–3194. [CrossRef]
23. Kinne, S.; Schulz, M.; Textor, C.; Guibert, S.; Balkanski, Y.; Bauer, S.E.; Berntsen, T.; Berglen, T.F.; Boucher, O.; Chin, M.; et al. An AeroCom initial assessment-Optical properties in aerosol component modules of global models. *Atmos. Chem. Phys.* **2006**, *6*, 1815–1834. [CrossRef]
24. Choobari, O.A.; Zawar-Reza, P.; Sturman, A. The global distribution of mineral dust and its impacts on the climate system: A review. *Atmos. Res.* **2014**, *138*, 152–165. [CrossRef]
25. Mahowald, N.; Albani, S.; Kok, J.F.; Engelstaeder, S.; Scanza, R.; Ward, D.S.; Flanner, M.G. The size distribution of desert dust aerosols and its impact on the Earth system. *Aeolian Res.* **2014**, *15*, 53–71. [CrossRef]
26. Evan, A.T.; Flamant, C.; Gaetani, M.; Guichard, F. The past, present and future of African dust. *Nature* **2016**, *531*, 493. [CrossRef]
27. Knippertz, P.; Todd, M.C. Mineral dust aerosols over the Sahara: Meteorological controls on emission and transport and implications for modeling. *Rev. Geophys.* **2012**, *50*. [CrossRef]
28. Haywood, J.M.; Francis, P.N.; Glew, M.D.; Taylor, J.P. The optical properties and direct radiative effect of Saharan Dust: A case study of two Saharan dust outbreaks using aircraft data. *J. Geophys. Res.* **2001**, *106*, 18417–18430. [CrossRef]
29. Dufresne, J.; Gautier, C.; Ricchiazzi, P.; Fouquart, Y. Longwave scattering effects of mineral aerosols. *J. Atmos. Sci.* **2002**, *59*, 1959–1966. [CrossRef]
30. Yoshioka, M.; Mahowald, N.M.; Conley, A.J.; Collins, W.D.; Fillmore, D.W.; Zender, C.S.; Coleman, D.B. Impact of desert dust radiative forcing on Sahel precipitation: Relative importance of dust compared to sea surface temperature variations, vegetation changes, and greenhouse gas warming. *J. Clim.* **2007**, *20*, 1445–1467. [CrossRef]
31. Alam, K.; Trautmann, T.; Blaschke, T.; Subhan, F. Changes in aerosol optical properties due to dust storms in the Middle East and Southwest Asia. *Remote Sens. Environ.* **2014**, *143*, 216–227. [CrossRef]
32. Asutosh, A.; Vinoj, V.; Murukesh, N.; Ramisetty, R.; Mittal, N. Investigation of June 2020 giant Saharan dust storm using remote sensing observations and model reanalysis. *Sci. Rep.* **2022**, *12*, 6114. [CrossRef] [PubMed]
33. Goudie, A.S.; Middleton, N.J. *Desert Dust in the Global System*; Springer Science & Business Media: Berlin/Heidelberg, Germany, 2006.
34. Marone, A.; Kane, C.T.; Mbengue, M.; Jenkins, G.S.; Niang, D.N.; Drame, M.S.; Gernand, J.M. Characterization of bacteria on aerosols from dust events in Dakar, Senegal, West Africa. *GeoHealth* **2020**, *4*, e2019GH000216. [CrossRef]
35. Guarnieri, M.; Balmes, J.R. Outdoor air pollution and asthma. *Lancet* **2014**, *383*, 1581–1592. [CrossRef]
36. Morman, S.A.; Plumlee, G.S. Dust and human health. In *Mineral Dust: A Key Player in the Earth System*; Knippertz, P., Stuut, J.-B.W., Eds.; Springer: Dordrecht, The Netherlands, 2014; pp. 385–409.
37. Diokhane, A.M.; Jenkins, G.S.; Manga, N.; Drame, M.S.; Mbodji, B. Linkages between observed, modeled Saharan dust loading and meningitis in Senegal during 2012 and 2013. *Int. J. Biometeorol.* **2016**, *60*, 557–575. [CrossRef]

38. Sultan, B.; Labadi, K.; Guegan, J.F.; Janicot, S. Climate drives the meningitis epidemics onset in West Africa. *PLoS Med.* **2005**, *2*, 43–49. [CrossRef]
39. Martiny, N.; Chiapello, I. Assessments for the impact of mineral dust on the meningitis incidence in West Africa. *Atmos. Environ.* **2013**, *70*, 245–253. [CrossRef]
40. Diokhane, A.M.; Sagna, P.; Diop, C.; Sambou, P.C.; Dioh, A.J.M.N. Importance of air quality degradation in Dakar in the first quarter of 2015: Explanatory elements. In Proceedings of the XXIXe Colloque de l'Association Internationale de Climatologie, Besançon, France, 6–9 July 2016.
41. Gasparrini, A.; Armstrong, B.; Kovats, S.; Wilkinson, P. The effect of high temperatures on cause-specific mortality in England and Wales. *Occup. Environ. Med.* **2012**, *69*, 56–61. [CrossRef] [PubMed]
42. Qian, Z.; He, Q.; Lin, H.M.; Kong, L.; Bentley, C.M.; Liu, W.; Zhou, D. High temperatures enhanced acute mortality effects of ambient particle pollution in the "oven" city of Wuhan, China. *Environ. Health Perspect.* **2008**, *116*, 1172–1178. [CrossRef] [PubMed]
43. World Health Organization (WHO). *Quantitative Risk Assessment of the Effects of Climate Change on Selected Causes of Death, 2030s and 2050s*; World Health Organization: Geneva, Switzerland, 2014.
44. Lelieveld, J.; Pozzer, A.; Pöschl, U.; Fnais, M.; Haines, A.; Münzel, T. Loss of life expectancy from air pollution compared to other risk factors: A worldwide perspective. *Cardiovasc. Res.* **2020**, *116*, 1910–1917. [CrossRef]
45. World Health Organization (WHO). *Air Pollution and Child Health: Prescribing Clean Air: Summary*; World Health Organization: Geneva, Switzerland, 2018.
46. Heft-Neal, S.; Burney, J.; Bendavid, E.; Burke, M. Robust relationship between air quality and infant mortality in Africa. *Nature* **2018**, *559*, 254–258. [CrossRef]
47. Toure, N.O.; Gueye, N.R.D.; Mbow-Diokhane, A.; Jenkins, G.S.; Li, M.; Drame, M.S.; Coker, K.A.R.; Thiam, K. Observed and modeled seasonal air quality and respiratory health in Senegal during 2015 and 2016. *GeoHealth* **2019**, *3*, 423–442. [CrossRef]
48. Valenzuela, A.; Costa, M.J.; Guerrero-Rascado, J.L.; Bortoli, D.; Olmo, F.J. Solar and thermal radiative effects during the 2011 extreme desert dust episode over Portugal. *Atmos. Environ.* **2017**, *148*, 16–29. [CrossRef]
49. Sousa, P.M.; Barriopedro, D.; Ramos, A.M.; García-Herrera, R.; Espírito-Santo, F.; Trigo, R.M. Saharan air intrusions as a relevant mechanism for Iberian heatwaves: The record-breaking events of August 2018 and June 2019. *Weather Clim. Extrem.* **2019**, *26*, 100224. [CrossRef]
50. Diba, I.; Basse, J.; Ndiaye, M.; Sabaly, H.N.; Diedhiou, A.; Camara, M. Potential dust induced changes on the seasonal variability of temperature extremes over the Sahel: A regional climate modeling study. *Front. Earth Sci.* **2021**, *8*, 591150. [CrossRef]
51. Niane, P.M.; Martiny, N.; Roucou, P.; Marilleau, N.; Janicot, S.; Gaye, A.T. Assessments for the Effect of Mineral Dust on the Spring Heat Waves in the Sahel. *Atmosphere* **2023**, *14*, 1373. [CrossRef]
52. Sambou, M.J.G.; Janicot, S.; Pohl, B.; Badiane, D.; Dieng, A.L.; Gaye, A. Heat wave occurrences over Senegal during spring: Regionalization and synoptic patterns. *Int. J. Climatol.* **2020**, *40*, 440–457. [CrossRef]
53. Roux, M.; Sagna, P. *Caractéristiques Climatiques*; Les éditions J.A.: Paris, France, 2007.
54. Beck, H.E.; Zimmermann, N.E.; McVicar, T.R.; Vergopolan, N.; Berg, A.; Wood, E.F. Present and future Köppen-Geiger climate classification maps at 1-km resolution. *Sci. Data* **2018**, *5*, 1–12. [CrossRef] [PubMed]
55. Almeida, S.P.; Casimiro, E.; Calheiros, J. Effects of apparent temperature on daily mortality in Lisbon and Oporto, Portugal. *Environ. Health* **2010**, *9*, 1–7. [CrossRef] [PubMed]
56. Diouf, S.; Deme, A.; Deme, E.H. Imputation methods for missing values: The case of Senegalese meteorological data. *Afr. J. Appl. Stat.* **2022**, *9*, 1245–1278.
57. Diouf, S.; Deme, A.; Deme, E.H.; Fall, P.; Diouf, I. An evaluation of the performance of imputation methods for missing meteorological data in Burkina Faso and Senegal. *Afr. J. Environ. Sci. Technol.* **2023**, *17*, 252–274.
58. Wallace, L. Intercomparison of PurpleAir sensor performance over three years indoors and outdoors at a home: Bias, precision, and limit of detection using an improved algorithm for calculating PM2.5. *Sensors* **2022**, *22*, 2755. [CrossRef]
59. Marticorena, B.; Chatenet, B.; Rajot, J.L.; Traore, S.; Coulibaly, M.; Diallo, A.; Koné, I.; Maman, A.; NDiaye, T.; Zakou, A. Temporal variability of mineral dust concentrations over West Africa: Analyses of a pluriannual monitoring from the AMMA Sahelian dust transect. *Atmos. Chem. Phys.* **2010**, *10*, 8899–8915. [CrossRef]
60. Marticorena, B.; Dorego, G.S.; Rajot, J.L.; Bouet, C.; Allègre, M.; Chatenet, B.; Féron, A.; Gaimoz, C.; Maisonneuve, F.; Siour, G.; et al. PM10 Concentration, Bambey, Senegal. [Dataset]. Aeris. Available online: https://indaaf.obs-mip.fr/indaaf-product/?uuid=0f546988-11fa-416e-a4c7-b8fcd7daebe6 (accessed on 13 February 2024). [CrossRef]
61. Holben, B.N.; Eck, T.F.; Slutsker, I.; Tanre, D.; Buis, J.P.; Setzer, A.; Vermote, E.; Reagan, J.A.; Smirnov, A. AERONET—A federated instrument network and data archive for aerosol characterization. *Remote Sens. Environ.* **1998**, *66*, 1–16. [CrossRef]
62. Inness, A.; Ades, M.; Agustí-Panareda, A.; Barré, J.; Benedictow, A.; Blechschmidt, A.-M.; Dominguez, J.J.; Engelen, R.; Eskes, H.; Flemming, J.; et al. The CAMS reanalysis of atmospheric composition. *Atmos. Chem. Phys.* **2019**, *19*, 3515–3556. [CrossRef]
63. Sow, B.; Tchanche, B.; Fall, I.; Souaré, S.; Mbow-Diokhané, A. Monitoring of atmospheric pollutant concentrations in the city of Dakar, Senegal. *Open J. Air Pollut.* **2021**, *10*, 18–30. [CrossRef]
64. Kaly, F.; Marticorena, B.; Chatenet, B.; Rajot, J.L.; Janicot, S.; Niang, A.; Yahi, H.; Thiria, S.; Maman, A.; Ndiaye, T.; et al. Variability of mineral dust concentrations over West Africa monitored by the Sahelian Dust Transect. *Atmos. Res.* **2015**, *164*, 226–241. [CrossRef]

65. Drame, M.S. Caractérisation et Impacts Climatiques des Aérosols en Afrique de l'Ouest. Ph.D. Thesis, Université Cheikh Anta Diop (UCAD), Dakar, Senegal, 2012.
66. Bado, N.; Ouédraogo, A.; Guengané, H.; Ky, T.S.M.; Bazyomo, S.D.; Korgo, B.; Dramé, M.S.; Sall, S.M.; Kieno, F.P.; Bathiebo, D.J. Climatological analysis of aerosols optical properties by airborne sensors and in situ measurements in west Africa: Case of the Sahelian zone. *Open J. Air Pollut.* **2019**, *8*, 118–135. [CrossRef]
67. Yarber, A.L.; Jenkins, G.S.; Singh, A.; Diokhane, A. Temporal relationships between Saharan dust proxies, climate, and meningitis in Senegal. *GeoHealth* **2023**, *7*, e2021GH000574. [CrossRef]
68. Carlson, T.N.; Prospero, J.M. The large-scale movement of Saharan air outbreaks over the northern equatorial Atlantic. *J. Appl. Meteorol.* **1972**, *11*, 283–297. [CrossRef]
69. Wu, C.; Li, K.; Bai, K. Validation and calibration of CAMS PM2.5 forecasts using in situ PM2.5 measurements in China and the United States. *Remote Sens.* **2020**, *12*, 3813. [CrossRef]
70. Ali, M.A.; Bilal, M.; Wang, Y.; Nichol, J.E.; Mhawish, A.; Qiu, Z.; Islam, M.N. Accuracy assessment of CAMS and MERRA-2 reanalysis PM2.5 and PM10 concentrations over China. *Atmos. Environ.* **2022**, *288*, 119297. [CrossRef]
71. Ukhov, A.; Mostamandi, S.; Da Silva, A.; Flemming, J.; Alshehri, Y.; Shevchenko, I.; Stenchikov, G. Assessment of natural and anthropogenic aerosol air pollution in the Middle East using MERRA-2, CAMS data assimilation products, and high-resolution WRF-Chem model simulations. *Atmos. Chem. Phys. Discuss.* **2020**, *2020*, 1–42. [CrossRef]
72. Royé, D.; Íñiguez, C.; Tobías, A. Comparison of air pollution–mortality associations using observed particulate matter concentrations and reanalysis data in 33 Spanish cities. *Environ. Health* **2024**, *2*, 161–169. [CrossRef]
73. Sekmoudi, I.; Khomsi, K.; Faieq, S.; Idrissi, L. Assessment of global and regional PM10 CAMSRA data: Comparison to observed data in Morocco. *Environ. Sci. Pollut. Res.* **2021**, *28*, 29984–29997. [CrossRef]
74. Pakszys, P.; Zielinski, T. Aerosol optical properties over Svalbard: A comparison between Ny-Ålesund and Hornsund. *Oceanologia* **2017**, *59*, 431–444. [CrossRef]
75. Knippertz, P.; Fink, A.H. Synoptic and dynamic aspects of an extreme springtime Saharan dust outbreak. *Q. J. R. Meteorol. Soc.* **2006**, *132*, 1153–1177. [CrossRef]
76. Grams, C.M.; Jones, S.C.; Marsham, J.H.; Parker, D.J.; Haywood, J.M.; Heuveline, V. The Atlantic inflow to the Saharan heat low: Observations and modelling. *Q. J. R. Meteorol. Soc.* **2010**, *136*, 125–140. [CrossRef]
77. Kante, I.K.; Badiane, D.; Sall, S.M.; Deme, A.; Diedhiou, A. Comparative study of the West African continental, coastal, and marine atmospheric profiles during the summer of 2006. *Int. J. Geophys.* **2012**, *2012*, 603949. [CrossRef]
78. Fawole, O.G.; Yusuf, N.; Sunmonu, L.A.; Obafaye, A.; Audu, D.K.; Onuorah, L.; Olusegun, C.F.; Deme, A.; Senghor, H. Impacts of COVID-19 restrictions on regional and local air quality across selected West African cities. *GeoHealth* **2022**, *6*, e2022GH000597. [CrossRef] [PubMed]
79. Kalu, A.E. The African dust plume: Its characteristics and propagation across West Africa in winter. In *Saharan Dust Mobilization, Transport, Deposition*; Morale, C., Ed.; Wiley: New York, NY, USA, 1979; pp. 95–118.
80. Schepanski, K.; Tegen, I.; Todd, M.C.; Heinold, B.; Bönisch, G.; Laurent, B.; Macke, A. Meteorological processes forcing Saharan dust emission inferred from MSG-SEVIRI observations of subdaily dust source activation and numerical models. *J. Geophys. Res. Atmos.* **2009**, *114*. [CrossRef]
81. Schepanski, K.; Tegen, I.; Macke, A. Saharan dust transport and deposition towards the tropical northern Atlantic. *Atmos. Chem. Phys.* **2009**, *9*, 1173–1189. [CrossRef]
82. Karyampudi, V.M.; Palm, S.P.; Reagan, J.A.; Fang, H.; Grant, W.B.; Hoff, R.M.; Moulin, C.; Pierce, H.F.; Torres, O.; Browell, E.V.; et al. Validation of the Saharan dust plume conceptual model using lidar, Meteosat, and ECMWF data. *Bull. Am. Meteorol. Soc.* **1999**, *80*, 1045–1076. [CrossRef]
83. Lavaysse, C.; Flamant, C.; Janicot, S.; Parker, D.J.; Lafore, J.-P.; Sultan, B.; Pelon, J. Seasonal evolution of the West African heat low: A climatological perspective. *Clim. Dyn.* **2009**, *33*, 313–330. [CrossRef]
84. Klose, M.; Shao, Y.; Karremann, M.K.; Fink, A.H. Sahel dust zone and synoptic background. *Geophys. Res. Lett.* **2010**, *37*, L09802. [CrossRef]
85. Mbourou, G.T.; Bertrand, J.J.; Nicholson, S.E. The diurnal and seasonal cycles of wind-borne dust over Africa north of the equator. *J. Appl. Meteorol. Climatol.* **1997**, *36*, 868–882. [CrossRef]
86. Bouniol, D.; Guichard, F.; Barbier, J.; Couvreux, F.; Roehrig, R. Sahelian heat wave characterization from observational data sets. *J. Geophys. Res. Atmos.* **2021**, *126*, e2020JD034465. [CrossRef]
87. Mallet, M.; Tulet, P.; Serça, D.; Solmon, F.; Dubovik, O.; Pelon, J.; Pont, V.; Thouron, O. Impact of dust aerosols on the radiative budget, surface heat fluxes, heating rate profiles and convective activity over west africa during march 2006. *Atmos. Chem. Phys.* **2009**, *9*, 7143–7160. [CrossRef]
88. Pagès, J.P.; Frangi, J.P.; Durand, P.; Estournel, C.; Druilhet, A. Étude de la couche limite de surface sahelienne—Experience yantala. *Bound.-Layer Meteorol.* **1988**, *43*, 183–203. [CrossRef]
89. Papachristopoulou, K.; Raptis, I.P.; Gkikas, A.; Fountoulakis, I.; Masoom, A.; Kazadzis, S. Aerosol optical depth regime over megacities of the world. *Atmos. Chem. Phys.* **2022**, *22*, 15703–15727. [CrossRef]
90. Camara, M.; Jenkins, G.; Konare, A. Impacts of dust on west african climate during 2005 and 2006. *Atmos. Chem. Phys. Discuss.* **2010**, *10*, 3053–3086.

91. Cowie, S.M.; Knippertz, P.; Marsham, J.H. A climatology of dust emission events from northern Africa using long-term surface observations. *Atmos. Chem. Phys.* **2014**, *14*, 8579–8597. [CrossRef]
92. Ozer, P. Les lithométéores en région Sahélienne. *Int. J. Trop. Ecol. Geogr.* **2001**, *24*, 1–317.
93. Jenkins, G.S.; McCauley, K.; Thompson, T.; Diokhane, A.M. WRF-CHEM Simulations of Unhealthy PM10 Concentrations During Four Dust Events in Senegal. *J. Geophys. Res. Atmos.* **2022**, *127*, e2022JD037068. [CrossRef]
94. To, T.; Stanojevic, S.; Moores, G.; Gershon, A.S.; Bateman, E.D.; Cruz, A.A.; Boulet, L.P. Global asthma prevalence in adults: Findings from the cross-sectional world health survey. *BMC Public Health* **2012**, *12*, 204. [CrossRef]